

## **UWL REPOSITORY**

**repository.uwl.ac.uk**

Modelling and Optimising the Performance of Graphene Oxide-Cu<sub>2</sub>SnS<sub>3</sub>-  
Polyaniline nanocomposite as an Adsorbent for Mercury Ion Removal

Enferadi, Sara, Eftekhari, Mohammad, Gheibi, Mohammad, Nabizadeh Moghaddam, Nikoo, Wacławek, Stanislaw and Behzadian, Kourosh ORCID: <https://orcid.org/0000-0002-1459-8408>  
(2024) Modelling and Optimising the Performance of Graphene Oxide-Cu<sub>2</sub>SnS<sub>3</sub>-Polyaniline nanocomposite as an Adsorbent for Mercury Ion Removal. Environmental Science and Pollution Research.

**This is the Accepted Version of the final output.**

**UWL repository link:** <https://repository.uwl.ac.uk/id/eprint/12004/>

**Alternative formats:** If you require this document in an alternative format, please contact: [open.research@uwl.ac.uk](mailto:open.research@uwl.ac.uk)

**Copyright:** Creative Commons: Attribution-No Derivative Works 4.0

Copyright and moral rights for the publications made accessible in the public portal are retained by the authors and/or other copyright owners and it is a condition of accessing publications that users recognise and abide by the legal requirements associated with these rights.

**Take down policy:** If you believe that this document breaches copyright, please contact us at [open.research@uwl.ac.uk](mailto:open.research@uwl.ac.uk) providing details, and we will remove access to the work immediately and investigate your claim.

# Modelling and Optimising the Performance of Graphene Oxide-Cu<sub>2</sub>SnS<sub>3</sub>-Polyaniline nanocomposite as an Adsorbent for Mercury Ion Removal

Sara Enferadi<sup>1</sup>, Mohammad Eftekhari<sup>2</sup>, Mohammad Gheibi<sup>3</sup>, Nikoo Nabizadeh Moghaddam<sup>1</sup>,  
Stanislaw Wacławek<sup>3</sup>, Kourosh Behzadian<sup>4\*</sup>

<sup>1</sup>Department of Chemistry, Faculty of Sciences, Ferdowsi University of Mashhad, Mashhad, Iran

<sup>2</sup>Department of Chemistry, Faculty of Sciences, University of Neyshabur, Neyshabur, Iran

<sup>3</sup>Institute for Nanomaterials, Advanced Technologies and Innovation, Technical University of Liberec, Studentská  
1402/2, 461 17 Liberec, Czech Republic

<sup>4</sup>School of Computing and Engineering, University of West London, St Mary's Rd, London, W5 5RF, UK

E-mail: [kourosh.behzadian@uwl.ac.uk](mailto:kourosh.behzadian@uwl.ac.uk)

## Abstract

Finding a cost-effective, efficient and environmentally friendly technique for removal of mercury ion (Hg<sup>2+</sup>) in water and wastewater can be a challenge task. This paper presents a novel and efficient adsorbent known as the Graphene oxide-Cu<sub>2</sub>SnS<sub>3</sub>-Polyaniline (GO-CTS-PANI) nanocomposite, which was synthesised and utilised to eliminate mercury ions (Hg<sup>2+</sup>) from water samples. The soft-soft interaction between Hg<sup>2+</sup> and sulfur atoms besides chelating interaction between -N and Hg<sup>2+</sup> and also electrostatic interaction are the main mechanisms for Hg<sup>2+</sup> adsorption onto the GO-CTS-PANI adsorbent. Various characterisation techniques, including Fourier transform infrared spectrophotometry (FT-IR), Field Emission Scanning Electron Microscopy (FESEM), Energy-dispersive X-ray spectroscopy (EDX), Elemental Mapping analysis, and X-ray diffraction analysis (XRD), were employed to analyse the adsorbent. The Box-Behnken method, utilising Design Expert Version 7.0.0, was employed to optimise the crucial factors influencing the adsorption process, such as pH, adsorbent quantity, and contact time. The results indicated that the most efficient adsorption occurred at pH 6.5,

with 12 mg of GO-CTS-PANI adsorbent, and a 30-minute contact time, achieving a maximum removal rate of 95% for 50 mg/L  $\text{Hg}^{2+}$  ions. The study also explored the isotherm and kinetics of the adsorption process, revealing that adsorption took place in sequential layers (Freundlich isotherm) and was followed by a physical interaction between the adsorbent and the adsorbate. The pseudo second-order kinetic equation proved to be a suitable model for interpreting the kinetic data. Furthermore, Response Surface Methodology (RSM) analysis indicated that pH was the most influential parameter in enhancing adsorption efficiency. In addition to traditional models, this study employed artificial intelligence methods, such as the Random Forest algorithm, to enhance the prediction of adsorption process efficiency. The findings demonstrated that the Random Forest algorithm exhibited high accuracy, achieving a correlation coefficient of 0.98. Overall, this research underscores the potential of the GO-CTS-PANI composite for effectively removing  $\text{Hg}^{2+}$  ions from water resources.

**Keywords:** *Adsorption, Artificial Intelligence, Graphene oxide- $\text{Cu}_2\text{SnS}_3$ -PANI, Mercury ion, Response Surface Methodology*

## **Introduction**

In the present era, addressing heavy metal pollution poses a significant challenge to environmental preservation (Briffa et al., 2020). One such hazardous metal is mercury ion ( $\text{Hg}^{2+}$ ), which exhibits toxicity even at low concentrations, leading to detrimental impacts on various bodily systems, including the nervous, digestive, immune, respiratory, and renal systems (Raj and Maiti 2019; Rice et al., 2014). The presence of  $\text{Hg}^{2+}$  in the environment is primarily attributed to human activities such as gold mining, alloy manufacturing, smelting, electricity and pesticide production, paint manufacturing, and waste incineration (Tchounwou et al., 2003; Mbanga et al., 2019; Streets et al., 2011). It infiltrates water resources through processes like atmospheric deposition, surface runoff, and direct discharge from industries and sewage treatment facilities. Once in water,  $\text{Hg}^{2+}$  can be converted into methylmercury by

bacteria, a highly toxic form of the element. Methylmercury accumulates in the food chain, particularly in aquatic organisms like fish, resulting in biomagnification and posing a health risk to humans when consumed (Global Mercury Assessment 2018; Yu et al., 2016). According to the recent Global Mercury Assessment, approximately 2000-2500 tonnes of mercury are released into the atmosphere, water, and soil each year (Global Mercury Assessment 2018). Consequently, the removal of  $\text{Hg}^{2+}$  from environmental water samples is of paramount importance.

Various techniques, including adsorption (Yu et al., 2016; Santana et al., 2016), membrane filtration (Albatrni et al., 2021; Yan et al., 2021), ion exchange (Han et al., 2020), and coagulation (Vasudevan et al., 2012), have been employed for this purpose. Among these, adsorption is the most commonly used method due to its inherent advantages, including the ease of preparing synthetic and natural adsorbents, relatively low cost, and high removal efficiency (Saadati et al., 2023; Rezazadeh et al., 2022; Wei et al., 2018; Li et al., 2014; Lei et al., 2014).

Graphene oxide (GO) is an oxidised form of graphene featuring oxygen-based functional groups that render it hydrophilic and readily dispersible in aqueous solutions. Its surface can be chemically or physically modified with various functional groups, making it suitable for a range of applications, including water treatment (Arshad et al., 2019; Amini-Fazl et al., 2021).

Ternary  $\text{Cu}_2\text{SnS}_3$  (CTS) is an environmentally friendly material with optoelectronic properties, well-suited for photoelectrochemical applications (Jathar et al., 2021). It also contains readily available elements, making it a cost-effective material (Berg et al., 2012). Furthermore, the presence of sulfur atoms (soft base) in CTS makes it an effective adsorbent for toxic soft heavy metals like  $\text{Hg}^{2+}$  (Velempini and Pillay 2019). Thus, the main purpose of the proposed method is to synthesise and characterise of GO-CTS-PANI nanocomposite to be used as an adsorbent that would maximise the efficiency of the removal of  $\text{Hg}^{2+}$  ions from water sample. This can

be achieved by synthesising CTS nanoplates and then its characterisation to modify GO followed by modification with PANI. Since CTS nanoplates have Sulphur atoms in its structure, it could be served as a suitable adsorbent for the removal of  $\text{Hg}^{2+}$  as a very toxic ion.

Hence, this study first aims to synthesise GO nanosheets using the Hummer method and modify them with CTS nanoplates and polyaniline (PANI) to create the GO-CTS-PANI nanocomposite. The synthesised adsorbent undergoes thorough characterisation using various techniques, including Fourier transform infrared spectrophotometry (FT-IR), Field Emission Scanning Electron Microscopy (FESEM), Energy-dispersive X-ray spectroscopy (EDX), Elemental Mapping analysis, and X-ray diffraction analysis (XRD). To determine the optimal conditions for achieving the maximum removal percentage (RP), the Box-Behnken experimental design is employed, and various isotherm and kinetic models are assessed and interpreted. Finally, both the Box-Behnken method and Random Forest algorithms are utilised for optimising and predicting the performance of the adsorption system, respectively.

## **Methodology**

This study is divided to different parts including experimental and numerical efforts which are demonstrated in **Figure 1**. According to the scheme, it can be found that experimental practices containing the characterisations and adsorption application process. Likewise, the numerical parts including classical computations for adsorption mechanism analysis, optimisation by Response Surface Methodology, and Machine Learning calculations.

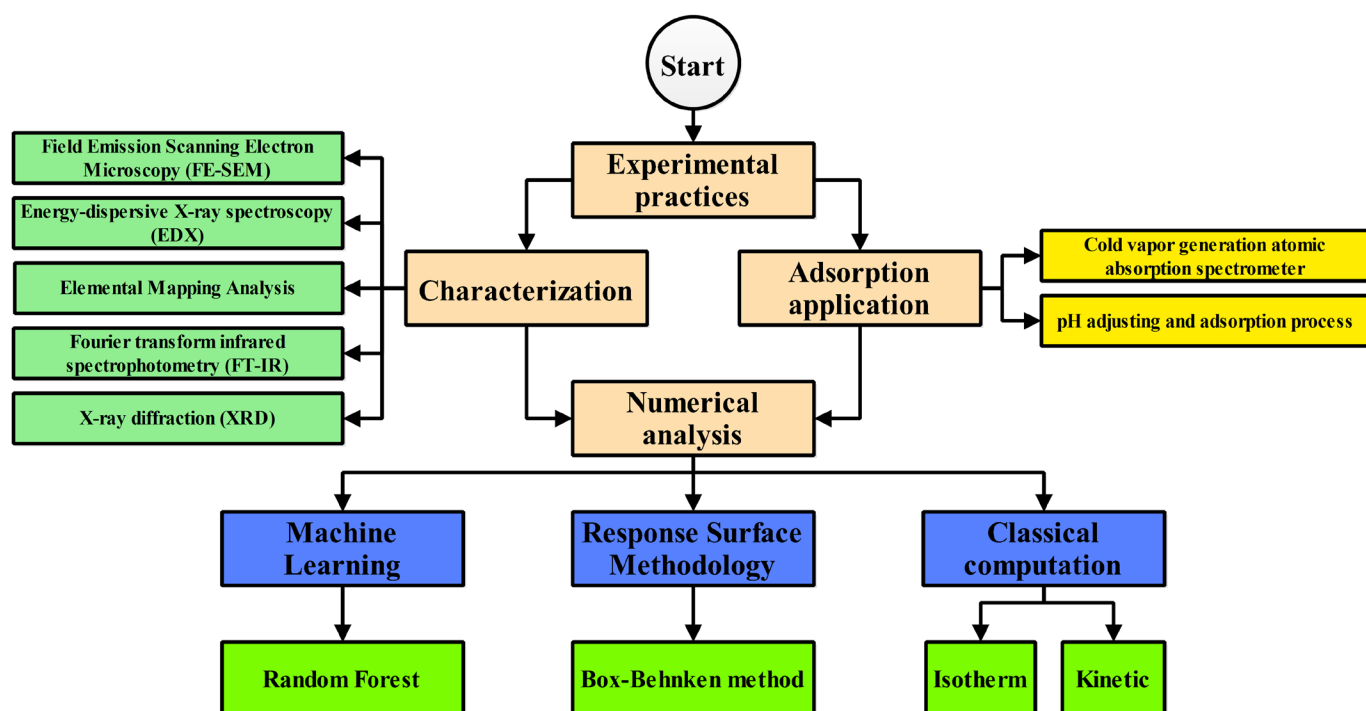


**Figure 1.** The research roadmap of this study.

## Instruments

FE-SEM, EDX, and Elemental Mapping Analysis were conducted using a BRNO-Mira3 LMU device manufactured by TESCAN in the Czech Republic. FT-IR analysis was performed with an AVATAR 370 spectrometer from the US, and XRD analysis utilized a D8-Advance Bruker Cu K $\alpha$ 1 instrument, also from the US. To determine the concentration of Hg<sup>2+</sup>, a cold vapor generation atomic absorption spectrometer (CV-AAS, Perkin Elmer Analyst 700, USA) equipped with a Hg hollow cathode lamp emitting at 253.7 nm was employed. pH adjustments were made with a Metrohm 827 pH-meter from Switzerland, and the separation of the

adsorbent from the solution was accomplished using an Andreas Hettich D72 centrifuge instrument from Germany.

## Reagents

The following reagents and chemicals were used in the experiment: Mercury nitrate monohydrate (Merck, Germany) to prepare a 1000 mg L<sup>-1</sup> Hg<sup>2+</sup> solution, Graphite, Cu(NO<sub>3</sub>)<sub>2</sub>·3H<sub>2</sub>O, SnCl<sub>2</sub>·2H<sub>2</sub>O, thiourea, aniline, ammonium persulfate, H<sub>2</sub>SO<sub>4</sub> (98.0%), KMnO<sub>4</sub> (99.0%), H<sub>2</sub>O<sub>2</sub> (30%), sodium borohydride (NaBH<sub>4</sub>, 99.0%) and HNO<sub>3</sub> (65.0%). All of these chemicals and reagents were also provided by Merck (Germany).

## Synthesis of GO-CTS-PANI nano-composite

### Synthesis of GO and CTS nanoplates

GO was synthesised using the Hummers method as described in **Figure 2** (Rezazadeh et al., 2022b). On the other hand, CTS was synthesised according to the following procedure: 0.241 g Cu(NO<sub>3</sub>)<sub>2</sub>·3H<sub>2</sub>O and 0.114 g SnCl<sub>2</sub>·2H<sub>2</sub>O were dissolved in 50 ml deionised water. Then 0.114 g thiourea was added to the mixture which causes to the formation of milky mixture. It was then stirred for 30 minutes and autoclaved at 180°C for 8 hours in a 100 mL Teflon-lined stainless-steel autoclave. The resulting CTS nanoplates washed with deionised water three times and dried overnight at 70 °C (Wang et al., 2017).

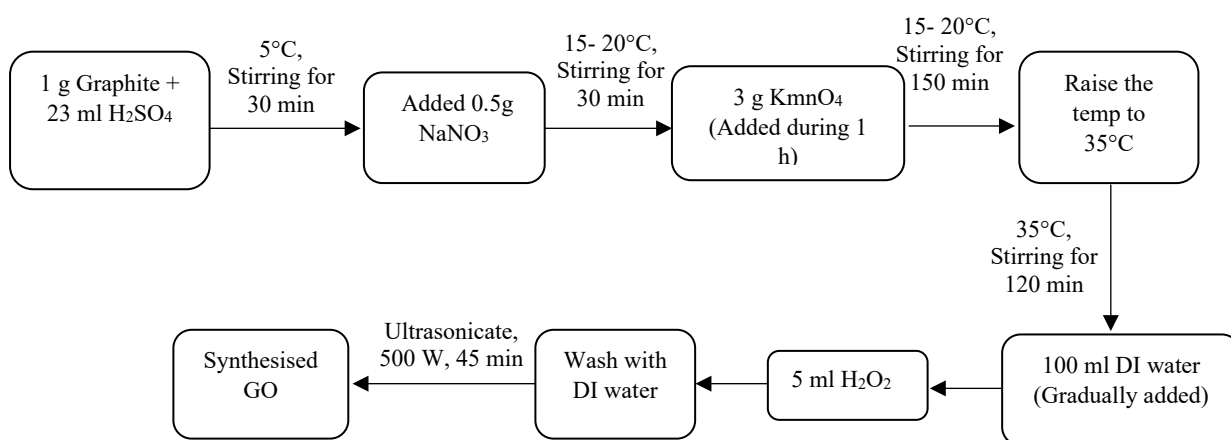


Figure 2. Synthetic route of GO in this study

## Synthesise of GO-CTS nanocomposite

To prepare the GO-CTS nanocomposite; 0.5 g of the synthesised GO in 100 ml deionised water (mixture 1) and 0.15g of CTS nanoplates in 50ml deionised water (mixture 2) were separately ultrasonicated for 45 minutes to obtain uniform mixtures. By addition of mixture 2 into the mixture 1, it was stirred for 6 hours at 400 rpm. The synthesised GO-CTS nanocomposite washed with deionised water three times and dried at 60 °C overnight.

## Synthesise of GO-CTS-PANI nanocomposite

In a solution containing 0.5 g of GO-CTS in 100 ml deionised water, 500 µL of aniline (in its monomeric form) was introduced and stirred for a duration of 10 minutes. Following this, 10 mL of a 1% ammonium persulfate solution was gradually incorporated into the mixture and stirred for a total of 10 h at 400 rpm. The resulting composite, known as GO-CTS-PANI nanocomposite, underwent multiple washes with deionized water and was subsequently dried overnight at 60 °C.

## Removal procedure

In a test solution with an initial  $\text{Hg}^{2+}$  concentration of 50 mg L<sup>-1</sup> at a pH of 6.5, 15 mg of GO-CTS-PANI was introduced, and the blend was agitated for a duration of 45 minutes. Subsequent to centrifugation for 5 min at 5000 rpm, the final concentration of  $\text{Hg}^{2+}$  at equilibrium was determined using CV-AAS. The removal percentage (RP) and the adsorption capacity ( $q_e$ ) were computed utilizing Equation (1) and (2), respectively.

$$\text{RP} = \frac{(C_0 - C_e)}{C_0} \times 100 \quad (1)$$

$$q_e = \frac{(C_0 - C_e) \times V}{m} \quad (2)$$

where  $C_e$  and  $C_0$  = equilibrium and initial concentration of  $\text{Hg}^{2+}$  in mg per litre, respectively.

$V$ = Sample volume in Lit,  $m$ = Adsorbent dosage in grams.



## Optimisation process

In order to enhance the efficiency of the experiment, a Box-Behnken design was utilized through Design Expert Version 7.0.0. The Box-Behnken design belongs to response surface methodology, which constructs a second-order polynomial equation to depict the connection between the influencing factors and the response variable. These influencing factors, encompassing pH, the quantity of adsorbent (M), and contact duration, were modified across three levels, resulting in a total of 15 experimental trials. The mathematical model derived from the Box-Behnken design is represented by Equation 3, as detailed in the work of Eftekhari et al. (2020).

$$Y = \beta_0 + \beta_1X_1 + \beta_2X_2 + \beta_3X_3 + \beta_{11}X_1^2 + \beta_{22}X_2^2 + \beta_{33}X_3^2 + \beta_{12}X_1X_2 + \beta_{13}X_1X_3 + \beta_{23}X_2X_3 \quad (3)$$

Herein, Y represents the response variable,  $\beta_0$  is the constant coefficient,  $\beta_1$ - $\beta_3$  are the linear coefficients and  $\beta_{11}$ ,  $\beta_{22}$ , and  $\beta_{33}$  are the quadratic coefficients. Moreover,  $\beta_{12}$ ,  $\beta_{13}$ , and  $\beta_{23}$  are the interaction coefficients.

In the optimisation process, the model performance is examined by desirability functions based on the most important features. The function involves transforming multiple response variables into a single scalar value between 0 and 1, where a value of 1 indicates the optimal condition for all response variables, and a value of 0 indicates the worst condition. The desirability function can be described as the result of multiplying individual desirability functions, with each individual function signifying the degree of desirability for a specific response variable. The allocation of weights for these functions is determined by considering the relative significance of each response variable in relation to the overall performance of the system, as outlined in the work by Eftekhari et al. (2020).

## Classical computations

The two-parameter isothermal equations represent mathematical formulas used to describe how adsorption capacity behaves under constant temperature conditions. Meanwhile, the three-parameter isothermal equations share similarities with the two-parameter equations but introduce an additional parameter to better capture the characteristics of the adsorption process (Eftekhari et al., 2020). Initially, the data is analysed using the two-parameter isotherm equations. If both the Langmuir and Freundlich models demonstrate similar performance, then the three-parameter equations are employed to precisely predict the adsorption mechanism (Eftekhari et al., 2020). In this research, both two-parameter models (Dubinin-Radushkevich, Temkin, Langmuir, and Freundlich) and three-parameter models (Toth, Khan, and Sips) are utilized to assess the adsorption mechanism. Furthermore, to evaluate the dynamic behavior of the adsorption process, several kinetic equations are applied (Eftekhari et al., 2020).

### **Machine Learning calculations**

In this current research, the Random Forest (RF) algorithm was employed to predict the removal percentage based on various influential factors, including pH, the quantity of adsorbent, and contact time. The RF algorithm is a machine learning technique that creates numerous decision trees during the training phase and outputs either the mode of the classes (for classification tasks) or the mean prediction (for regression tasks) from the individual trees. In this specific study, the RF algorithm was trained using a dataset comprising known removal percentages and their corresponding influential factors. Additionally, to ensure the accuracy and robustness of the model, the optimal K-fold value was fine-tuned (Eftekhari et al., 2021). The K-fold technique is a method for validating a model, involving the division of the dataset into K equally sized subsets or folds. The model is trained on K-1 folds and tested on the remaining fold, with this process repeated K times. The model's performance is then averaged across the K folds to provide an estimate of its accuracy. In this study, the optimal K value was

determined by adjusting the parameter through a grid search approach (Eftekhari et al., 2021).

The mathematical representation of the RF algorithm can be found in Equation 4.

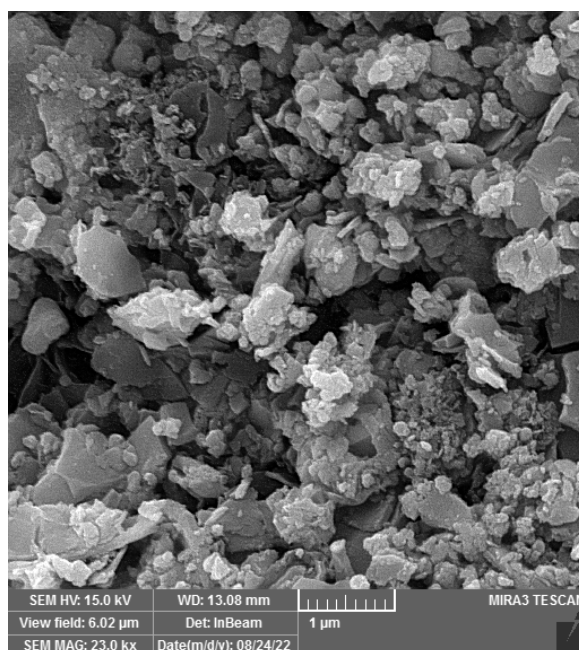
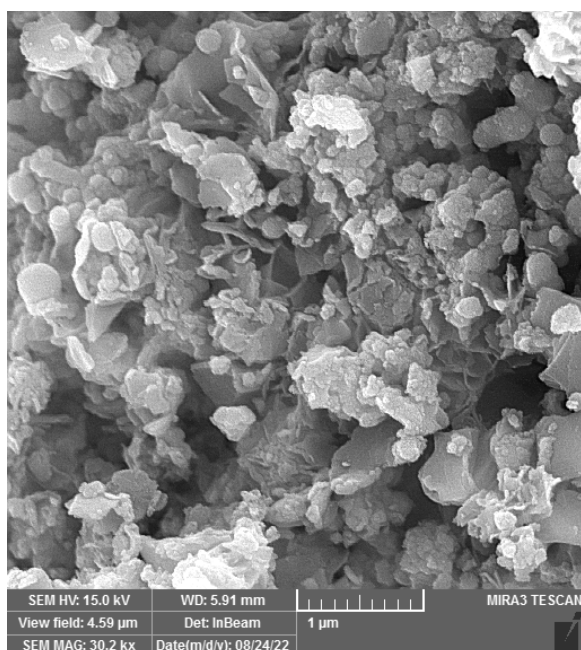
Given a training set  $T = \{(x_1, y_1), (x_2, y_2), \dots, (x_n, y_n)\}$  (4)

In the context of this equation where " $x_i$ " represents the influential factors and " $y_i$ " stands for the corresponding removal percentage, the RF algorithm generates a diverse set of decision trees denoted as " $T_i$ " by employing bootstrap aggregating, commonly referred to as "bagging," on the training dataset " $T$ " (Eftekhari et al., 2021). The result produced by the RF algorithm corresponds to the class that emerges as the mode among the classes (for classification tasks) or the mean prediction (for regression tasks) from the individual decision trees. All computational tasks and model training were carried out using WEKA 3.9.

## **Results and Discussion**

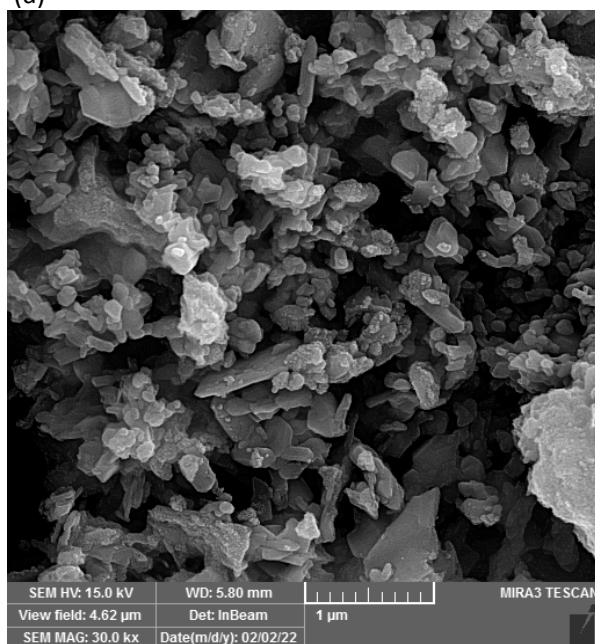
### **Characterisation of CTS nanoplates and GO-CTS-PANI composite**

The CTS nanoplates were synthesised and characterised using XRD, FESEM, and EDX analysis. FESEM images of the synthesised CTS nanoplates are shown in **Figure 3**, while the EDX spectrum presented in **Figure 4** confirms the high purity of CTS nanoplates with peaks corresponding to Cu (0.93 and 8.04 keV), Sn (3.44 keV) and S (2.31 keV). XRD patterns of the synthesised CTS nanoplates are illustrated in **Figure 5**, which shows major diffraction peaks appearing at  $2\theta = 28.5^\circ, 32.8^\circ, 47.5^\circ, 56.4^\circ$  and  $68.6^\circ$ . These peaks correspond to (111), (200), (220), (311) and (400) of CTS (JCPDS no. 89-2877), indicating the CTS nanoplates possess a cubic phase (Zaman and Poolla 2020).



(a)

(b)



(c)

**Figure 3. FESEM images of CTS nanoplates (a-c)**

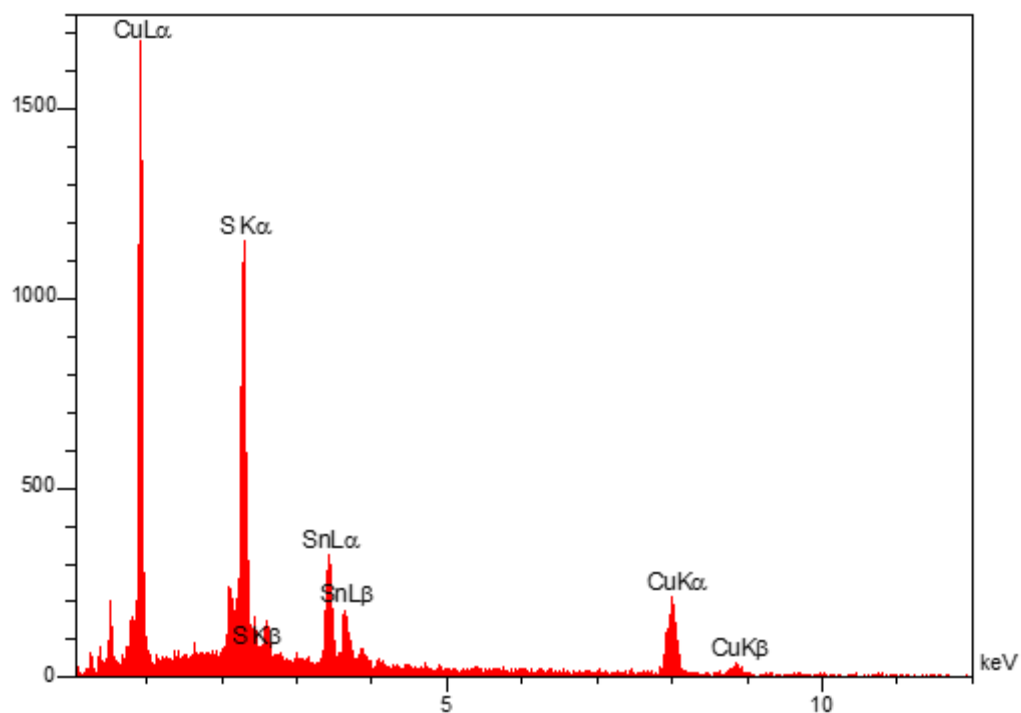


Figure 4. EDX analysis of CTS nanoplates

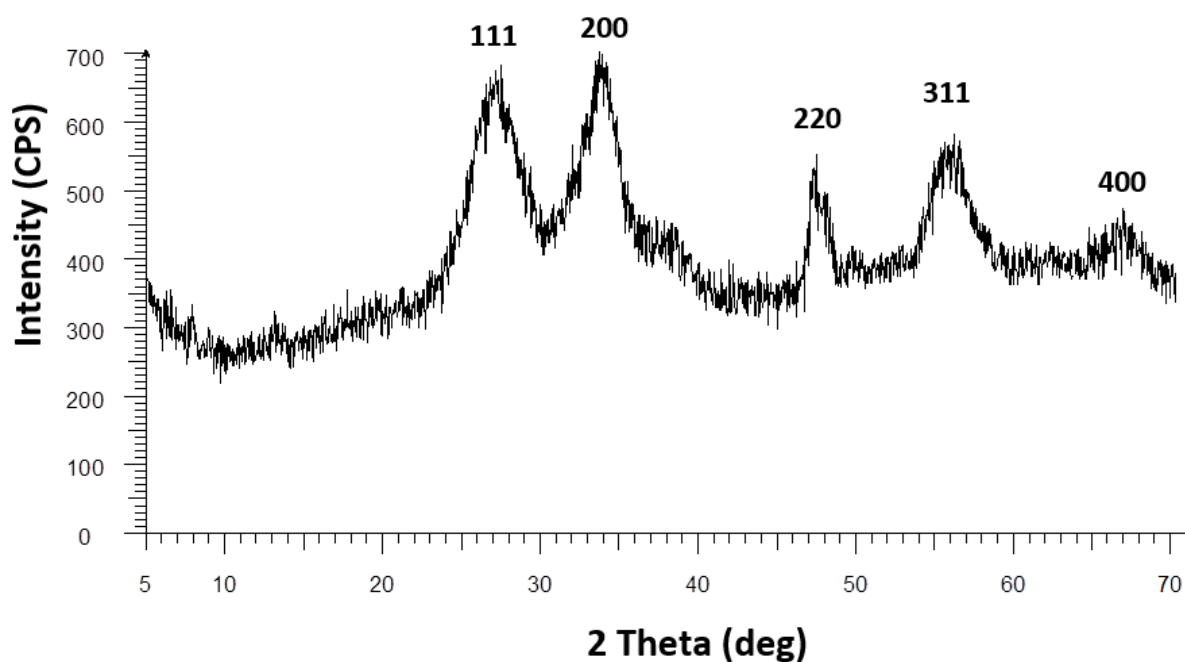
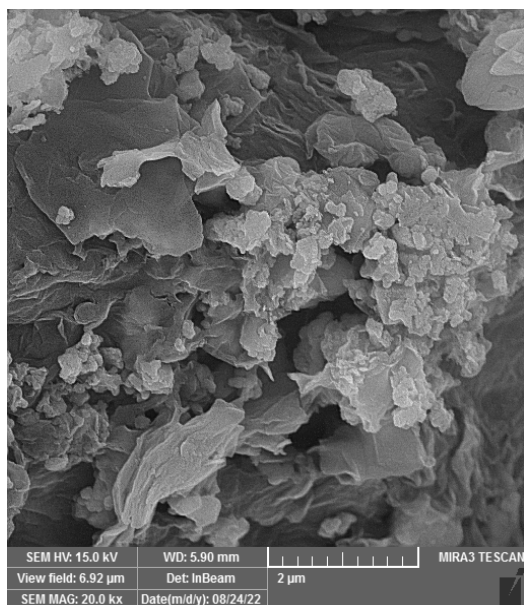
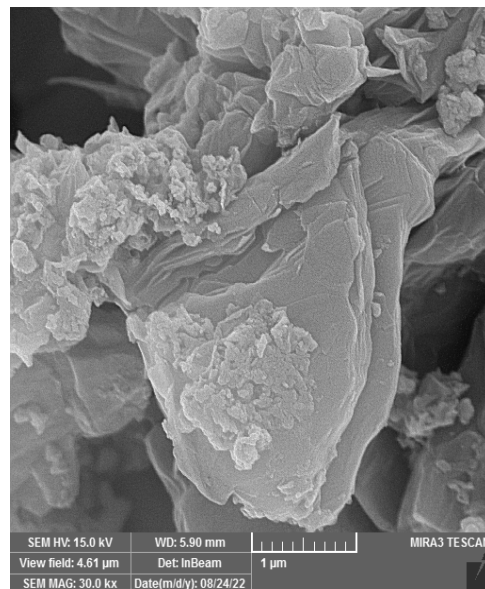


Figure 5. XRD spectrum of CTS nanoplates

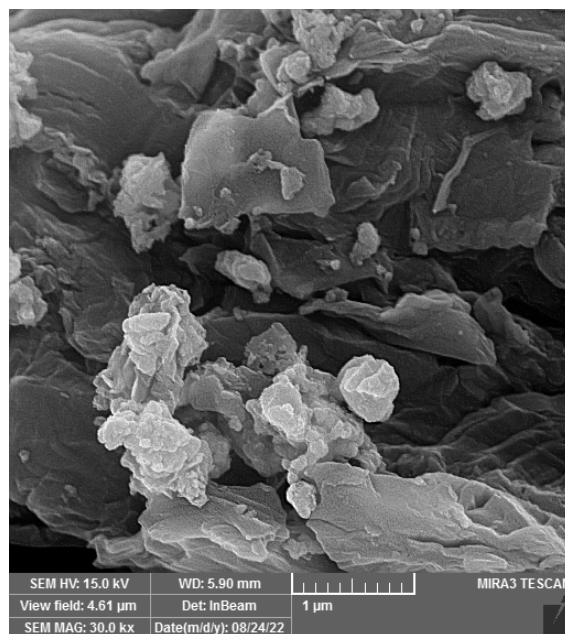
**Figure 6** presents FESEM images of GO-CTS-PANI composite, which indicates that GO nanosheets are occupied by CTS nanoplates and PANI. EDX analysis of the composite in **Figure 7** also shows the presence of N and O groups at 0.39 and 0.52 eV, respectively, which are attributed to PANI and GO in the synthesised composite.



(a)



(b)



(c)

**Figure 6. FESEM images of GO-CTS-PANI nanocomposite**

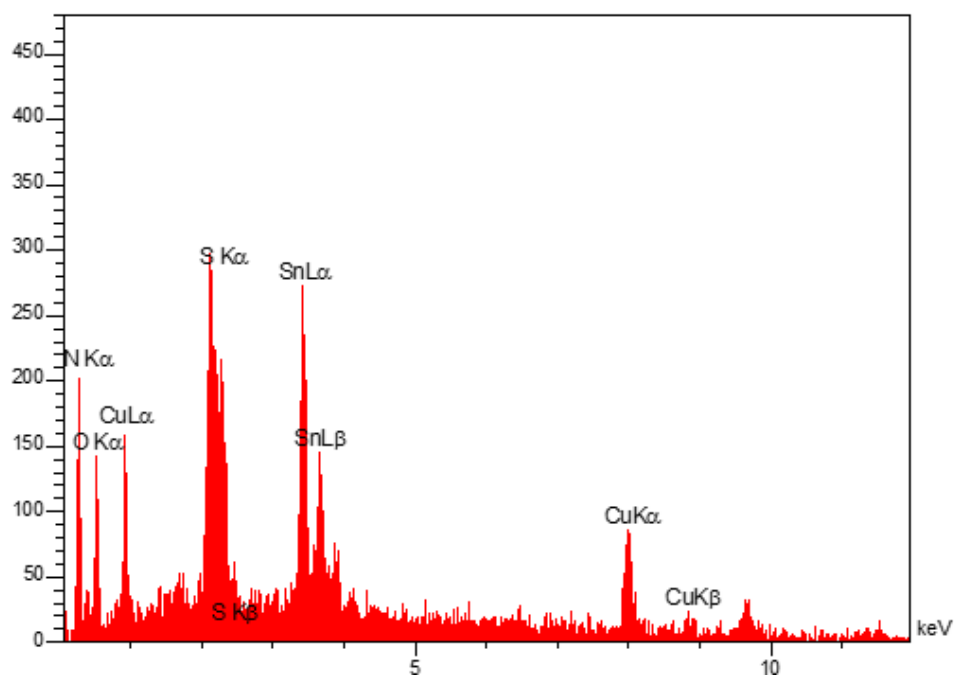
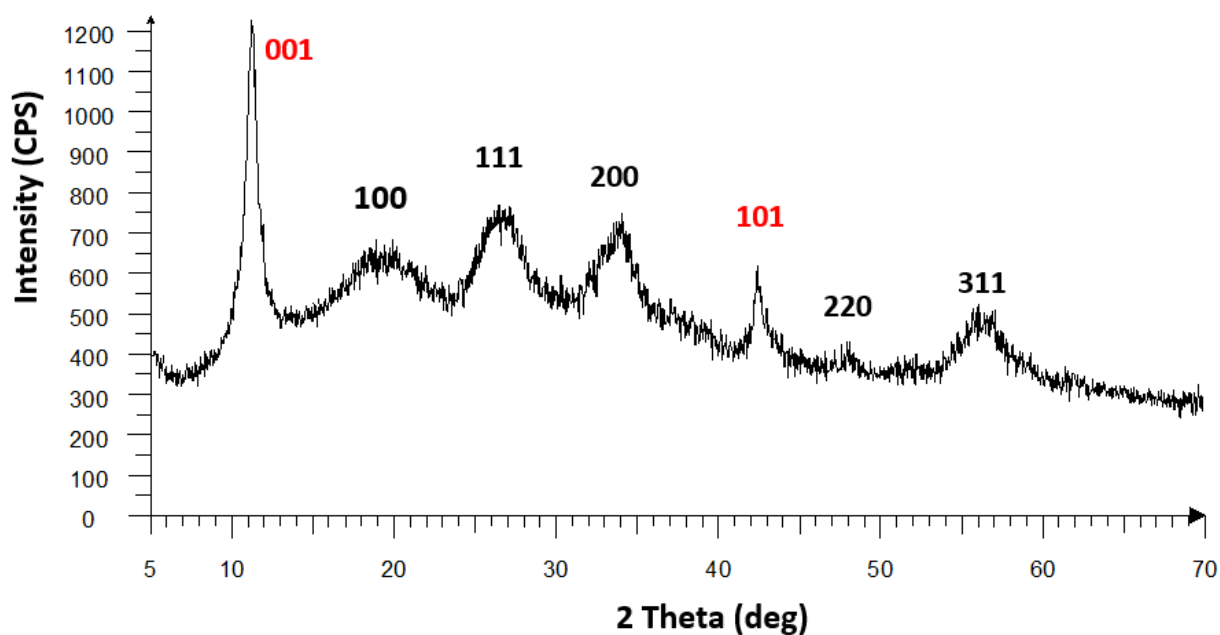


Figure 7. EDX analysis of GO-CTS-PANI composite

The GO-CTS-PANI composite was analysed using XRD in **Figure 8**. The analysis revealed clear appearance of the main peaks of CTS nanoplates in the spectrum. In addition, two peaks of GO at  $2\theta = 11.6^\circ$  and  $42.5^\circ$  correspond to (001) and (101), respectively (Shabani-Nooshabadi and Zahedi 2019) while a broad peak at  $2\theta=20^\circ$  corresponds to (100) and attributed to PANI (Liu et al., 2018).

243



244

245

Figure 8. XRD spectrum of GO-CTS-PANI nanocomposite

246

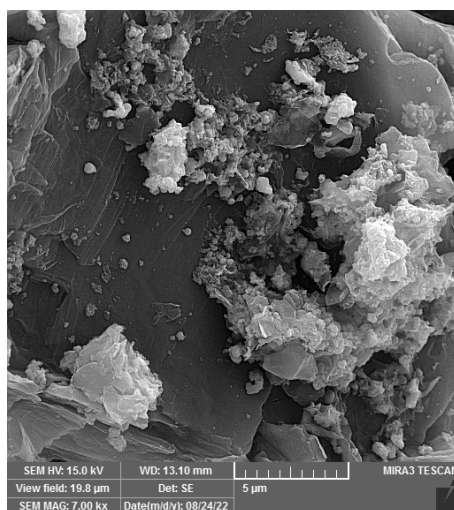
MAP analysis was conducted on GO-CTS-PANI nanocomposite, and the results (Figure 9a-

247

e) revealed that C (7a), Cu (7b), N(7c), O(7d), S(7e) and Sn (7f) are the main components of

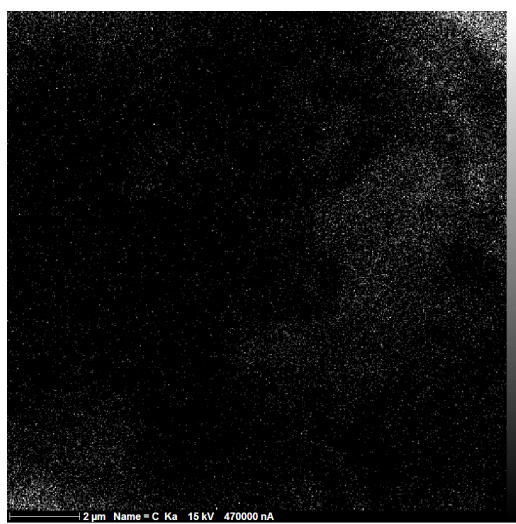
248

the synthesised GO-CTS-PANI nanocomposite.



(a)

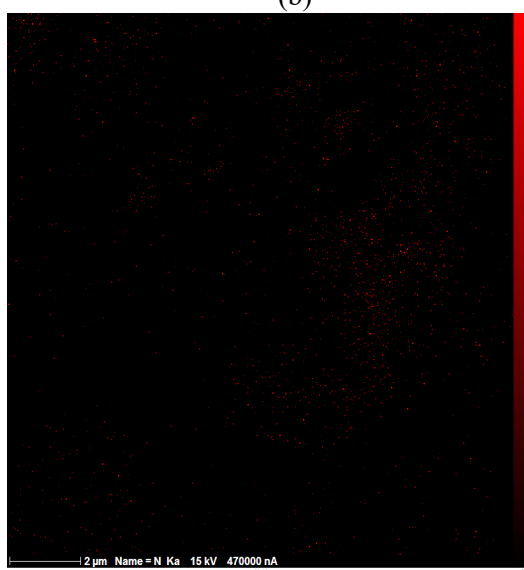




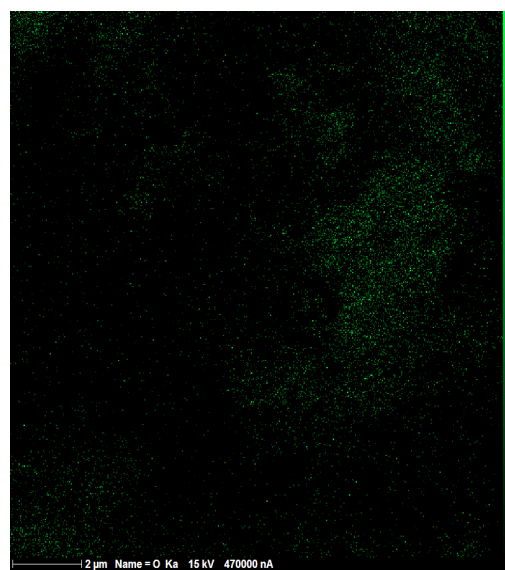
(b)



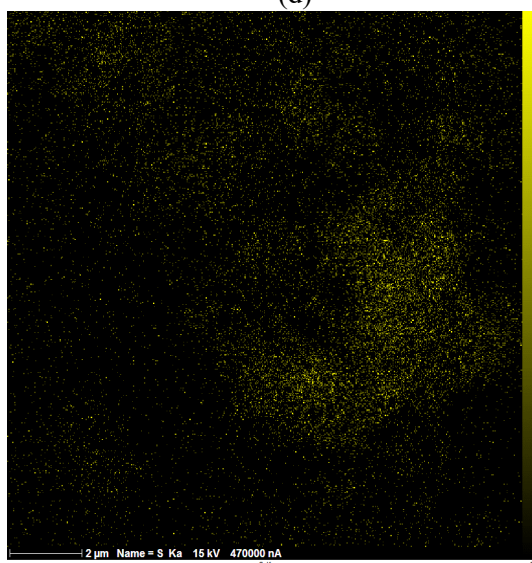
(c)



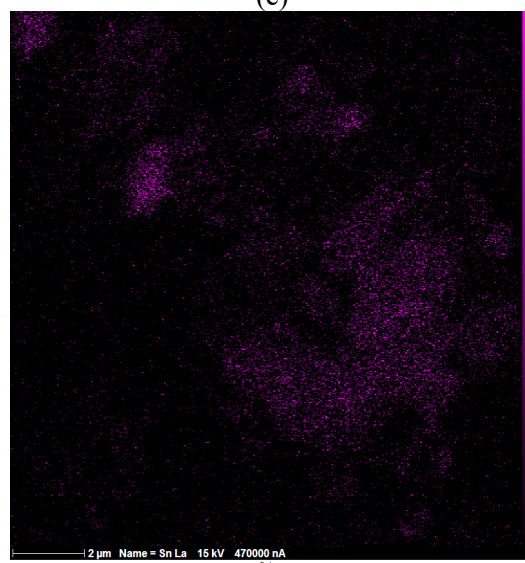
(d)



(e)



(f)



(g)

Figure 9. MAP elemental analysis of GO-CTS-PANI; distribution of mapping zone in SEM image (a) C

(b), Cu (c), N(d), O(e), S(f) and Sn (g) (a-f images).

Finally, the FT-IR spectra of GO-CTS-PANI composite and CTS nanoplates are presented in **Figure 10**. The CTS spectrum shows a sharp peak at 500-750  $\text{cm}^{-1}$  that is related to the vibration of Cu-S, Sn-S bonds. The band at 1630  $\text{cm}^{-1}$  is due to the O-H bending of water molecules and a peak appeared at 1130  $\text{cm}^{-1}$  could be attributed to the stretching vibration of C-N band of thiourea in the structure of CTS nanoplates. The FT-IR spectrum of GO-CTS-PANI shows the peaks at 3300  $\text{cm}^{-1}$  (stretching of N-H, O-H), 1050  $\text{cm}^{-1}$  (C-O of hydroxyl group), 1730  $\text{cm}^{-1}$  (C=O) and 1650  $\text{cm}^{-1}$  (C=C). Moreover, the intense peak of Cu-S and Sn-S (at 500-750  $\text{cm}^{-1}$ ) in CTS nanoplates is reduced after modification by GO-PANI.

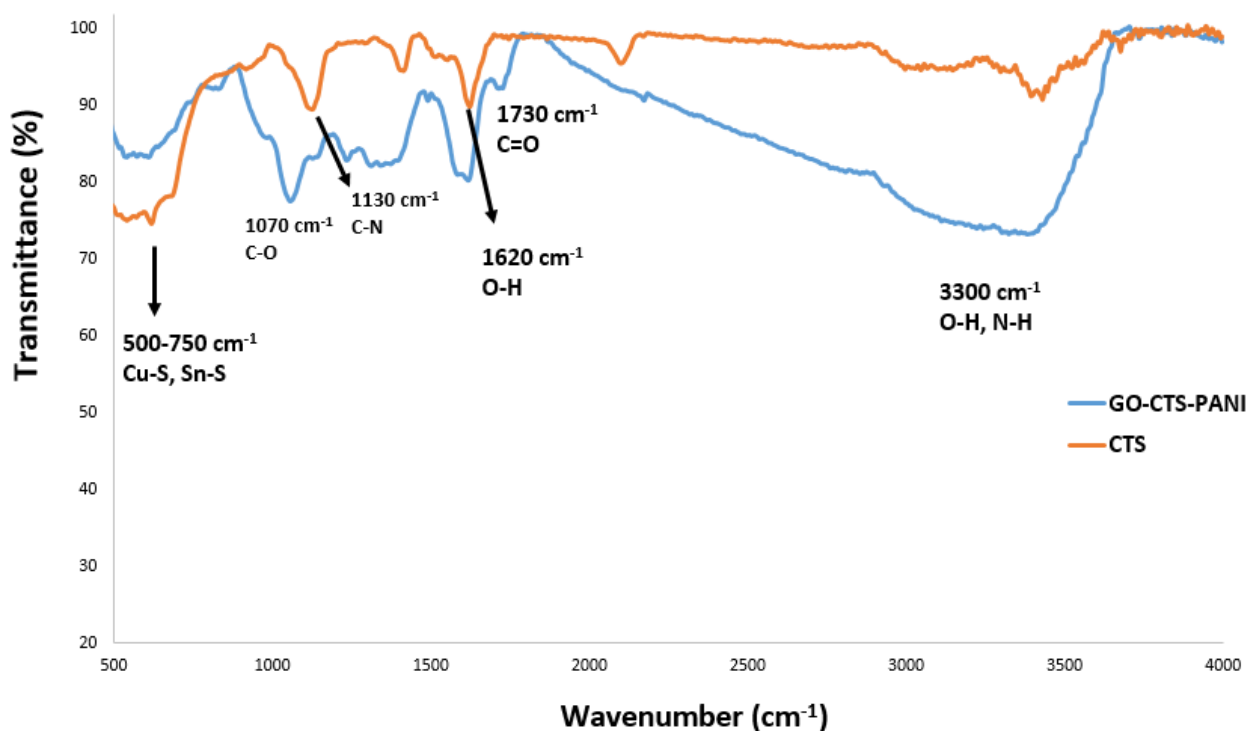


**Figure 10. FT-IR spectrum of the synthesised CTS nanoplates and GO-CTS-PANI**

### Optimisation of parameters

To optimise effective features including pH, adsorbent amount (M), and contact time, Box-Behnken method was applied using Design Expert Version 7.0.0 for 50  $\text{mg L}^{-1}$   $\text{Hg}^{2+}$  ion. The

range of each parameter in the Design of Experiments (DOE) as well as the statistical analysis outcomes of experiments are presented in Table 1. The responses obtained from the experiments are distributed between 36% and 95%. Also, the model follows polynomial and quadratic equation for fitting effective features as per removal percentage of  $Hg^{2+}$ . Likewise, according to Table 1, it can be concluded that there is spread distribution of  $Hg^{2+}$  ion purification from water samples in different conditions of adsorption operation process. Therefore, finding the optimum condition will be valuable in viewpoints of water treatment efficiency.

**Table 1. The limitations of DOE in this study**

Factor	Name	Units	Type	Low Actual	High Actual	Low Coded	High Coded	Mean	Std. Dev.	
A	pH		Numeric	2	7	-1	1	4.5	1.714986	
B	M	mg	Numeric	5	15	-1	1	10	3.429972	
C	Contact time	min	Numeric	10	50	-1	1	30	13.71989	
Response	Name	Units	Obs	Analysis	Minimum	Maximum	Mean	Std. Dev.	Ratio (max/min)	Model
Y1	RP	%	17	Polynomial	36	95	59.47059	17.9	2.58	Quadratic

Table 2 displays various statistical metrics, including Standard Deviation, R-Squared, Adjusted R-Squared, Predicted R-Squared, and Press, for four distinct models: linear, 2FI, quadratic, and cubic. As indicated by the information in Table 2, the quadratic model (as described in Equation 3) exhibits superior performance, with an R-Squared value of 0.99 and a Predicted R-Squared value of 0.94, outperforming the other models. Nevertheless, it's worth noting that the Predicted R-Squared value can be further enhanced by incorporating machine learning computations.

284

Table 2. The curve fitting regression outcomes in different mathematical models.

Source	Std. Dev.	R-Squared	Adjusted R-Squared	Predicted R-Squared	PRESS	
Linear	7.412232	0.869001	0.838771	0.741765587	1407.955	
2FI	8.351559	0.872074	0.795318	0.409168432	3221.353	
Quadratic	2.339108	0.992975	0.983944	0.942684058	312.5	Suggested
Cubic	2.280351	0.996185	0.98474			

285

$$286 \quad \text{RP} = -3.38 - 2.36 * \text{pH} + 5.82 * \text{M} + 1.07 * \text{Contact time} + 0.14 * \text{pH} * \text{M} + 0.015 * \text{pH} * \text{Contact} \\ 287 \quad \text{time} + 7.5\text{E-}003 * \text{M} * \text{Contact time} + 1.12 * \text{pH}^2 - 0.29 * \text{M}^2 - 0.018 * \text{Contact time}^2$$

288

(3)

289 The Analysis of Variance (ANOVA) results presented in Table 3 demonstrates that the  
 290 designed model (Equation 1) is significant with a P-value <0.0001 and the error value in  
 291 prediction (lack of fit) is insignificant indicating the validity of the equation. Among the three  
 292 parameters (pH, M, and contact time), pH has the smallest P-value (<0.0001) and largest F-  
 293 value (842.19). Between the other two factors, the mass of adsorbent has more importance (P-  
 294 value = 0.0039) that the contact time (P-value = 0.0462).

295

Table 3. The results of ANOVA practices in this study

Source	Sum of Squares	Mean Square	F-Value	P-value	
Model	5413.9	601.54	109.9436	< 0.0001	significant
A-pH	4608	4608	842.1932	< 0.0001	
B-M	98	98	17.91123	0.0039	
C-Contact time	32	32	5.848564	0.0462	
AB	12.25	12.25	2.238903	0.1782	
AC	2.25	2.25	0.411227	0.5418	
BC	2.25	2.25	0.411	0.5418	
A^2	207.79	207.79	37.97	0.0005	
B^2	235.26	235.26	42.99	0.0003	
C^2	235.26	235.26	42.99	0.0003	
Residual	38.3	5.47			
Lack of Fit	17.5	5.83	1.12	0.4395	not significant
Pure Error	20.8	5.2			
Cor Total	5452.2				

The statistical distribution of results is presented in **Figure 11** (Normal% probability via internally studentised residuals). Based on the results the normality of experimental outputs of the DOE were found to be normal all the data are located within the normal diagram according to the declared scheme. A normally distributed dataset implies that the mean and standard deviation of the data are well-defined, which can aid in the design and optimisation of the system. Additionally, engineers can use this information to make informed decisions about the system, such as setting appropriate tolerances for manufacturing processes or determining the expected variability in system performance. Overall, the normality of the experimental outputs is a useful piece of information for engineers to consider when analysing and designing systems. **Figure 12(a-c)** shows the outcomes of the dual sensitive evaluation of effective experimental factors for adsorption of  $\text{Hg}^{2+}$  onto GO-CTS-PANI. **Figure 12a** demonstrates the influence of pH and amount of adsorbent on the recovery percentage of  $\text{Hg}^{2+}$ .

The findings suggest that elevating the pH level results in an augmentation of the removal percentage (RP) of  $\text{Hg}^{2+}$ , reaching its peak effectiveness at around pH 6.5-7. This notable enhancement in RP as pH increases is likely attributed to the deprotonation of functional groups like carboxyl, sulfur, and N-H on the adsorbent, enhancing their interaction with  $\text{Hg}^{2+}$  (Anirudhan et al., 2015; Gao et al., 2021). Conversely, the lower RP of  $\text{Hg}^{2+}$  in acidic solutions (pH<5) is linked to the protonation of S-atoms in CTS nanoplates, protonation of hydroxyl groups, incomplete dissociation of carboxylic acid groups (which have pKa values around 5) on GO, and protonation of -NH groups on PANI, leading to electrostatic repulsion between  $\text{Hg}^{2+}$  ions. Within the pH range of 6–7,  $\text{Hg}^{2+}$  predominantly exists as  $\text{Hg}(\text{OH})_2$  (approximately 79%) and  $\text{HgOH}^+$  (approximately 10%) (Anirudhan and Shainy 2015). According to the Pearson rule, interactions are more favourable between hard acids and hard bases, and soft acids and soft bases (Santhana Krishna Kumar et al., 2013). Additionally, considering that neutral molecules are softer acids compared to metal cations, the interaction between  $\text{Hg}^{2+}$

species becomes more favourable at higher pH values. Regarding the influence of the parameter "M" on RP, an increase in "M" enhances the RP of  $\text{Hg}^{2+}$  because it provides more available active sites for interaction with the analyte. However, a further increase in the "M" parameter eventually diminishes the RP, primarily due to the aggregation of the adsorbent (Eftekhari et al., 2020). **Figures 12b and 12c** depict the effects of contact time, "M," and pH on the RP of  $\text{Hg}^{2+}$ , with the results showing that an extended contact time leads to an improved RP of  $\text{Hg}^{2+}$ . **Figure 13** shows the EDX spectrum of GO-CTS-PANI adsorbent after adsorption of  $\text{Hg}^{2+}$  that shows a peak of the adsorbed  $\text{Hg}^{2+}$  at 9.9 keV. The obtained results clearly shows that  $\text{Hg}^{2+}$  ions effectively adsorbed onto the GO-CTS-PANI adsorbent.

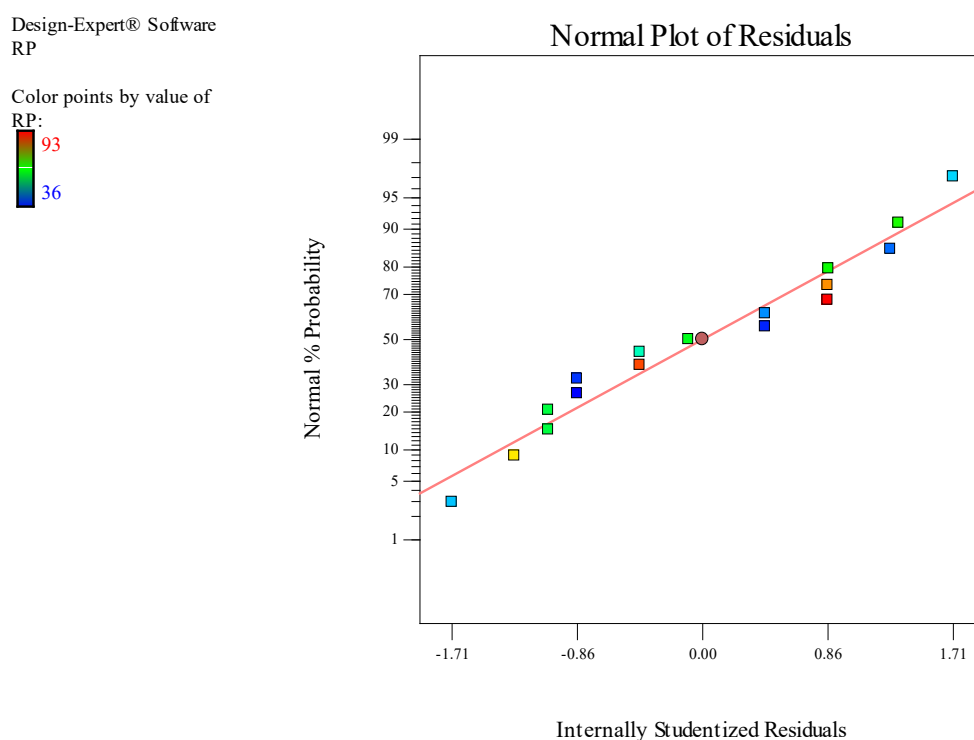


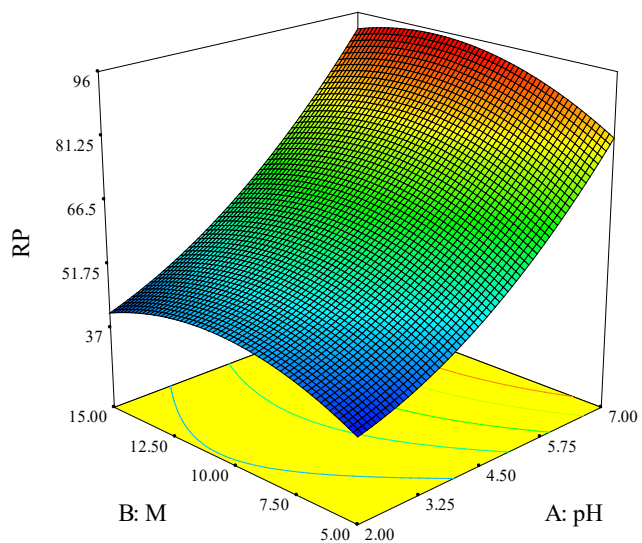
**Figure 11. The normal distribution of experimental outcomes in this study**

Design-Expert® Software



X1 = A: pH  
X2 = B: M

Actual Factor  
C: Contact time = 30.00



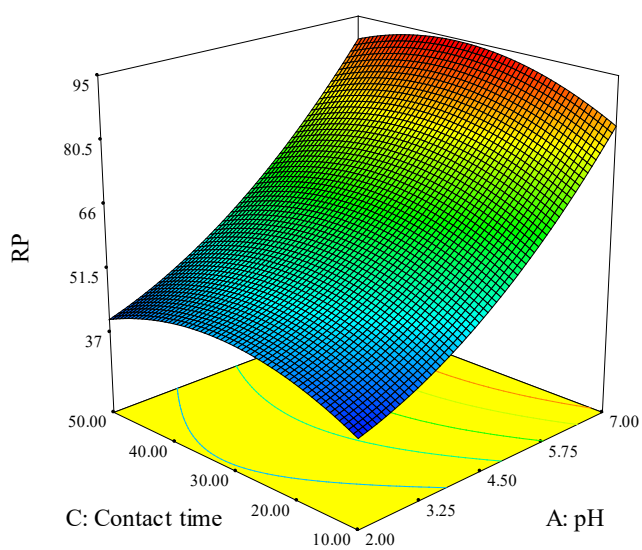
(a)

Design-Expert® Software



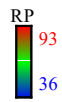
X1 = A: pH  
X2 = C: Contact time

Actual Factor  
B: M = 10.00



(b)

Design-Expert® Software

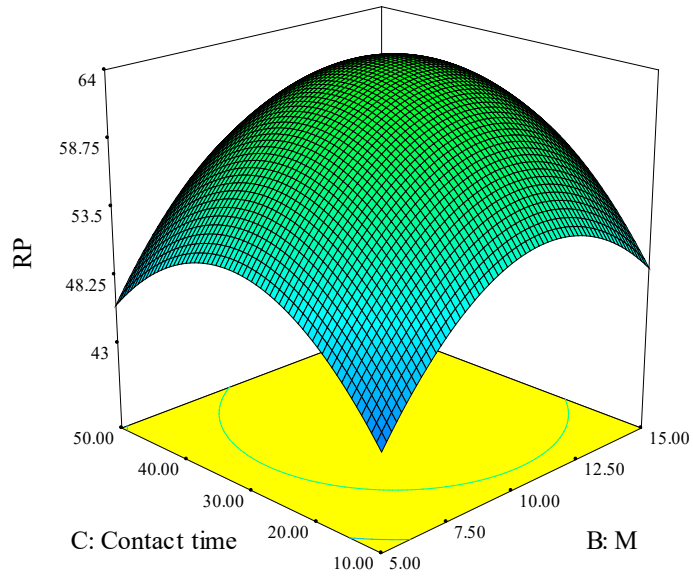


X1 = B: M

X2 = C: Contact time

Actual Factor

A: pH = 4.50



(c)

Figure 12. The sensitive analysis of the studied parameters on RP of  $\text{Hg}^{2+}$  ( $50 \text{ mg L}^{-1}$ ) (a-c).

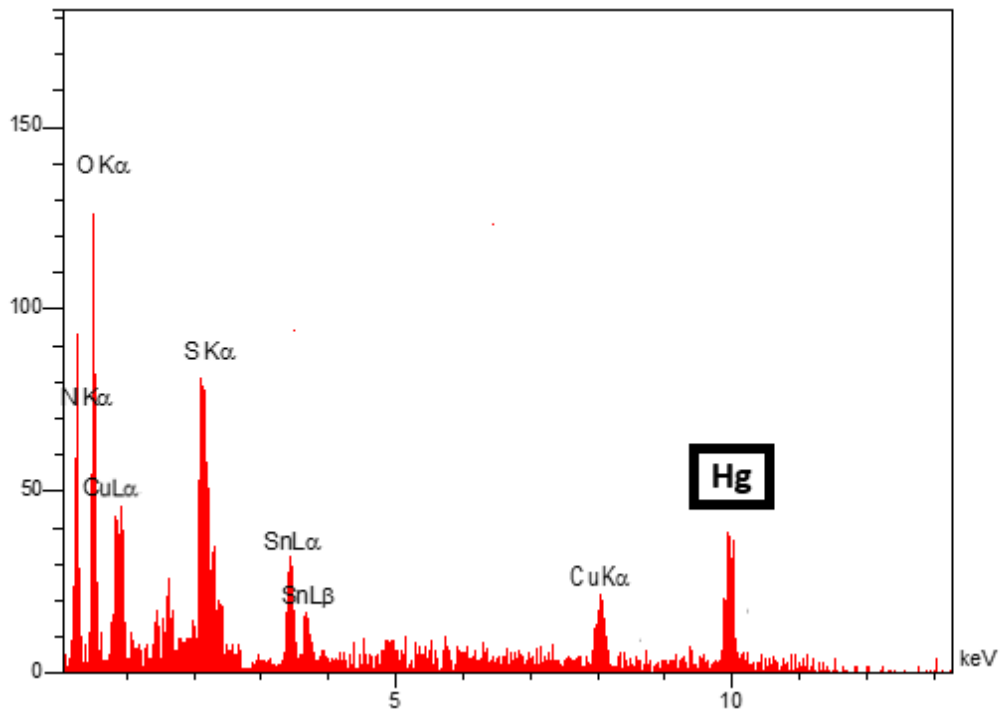


Figure 13. EDX analysis of GO-CTS-PANI after adsorption of  $\text{Hg}^{2+}$  ions.



After conducting sensitive analysis and mathematical modelling using Box-Behnken model, the optimal values of the effective factors are computed. The results (Table 4) show that the maximum performance (removal percentage as RP) for removing  $\text{Hg}^{2+}$  from water samples using GO-CTS-PANI is 95%, indicating the best operational efficiency. Therefore, the optimal performance can be obtained based on optimal features of pH of 6.5, M=12 mg and contact time of 30 min. These effective features are also depicted in **Figure 14** based on the desirability. The contours in the figure show that the maximum desirability for predicting the optimal conditions is achieved with high levels of pH and intermediate values of M.

**Table 4. The optimal suggestions of effective features based on RP% in this study.**

pH	M (mg)	Contact time (minutes)	RP (%)	Desirability
6.59	10.39	40.59	97	1.000
6.56	10.42	39.18	97.6633	1.000
6.50	12.07	30.38	98.3089	1.000

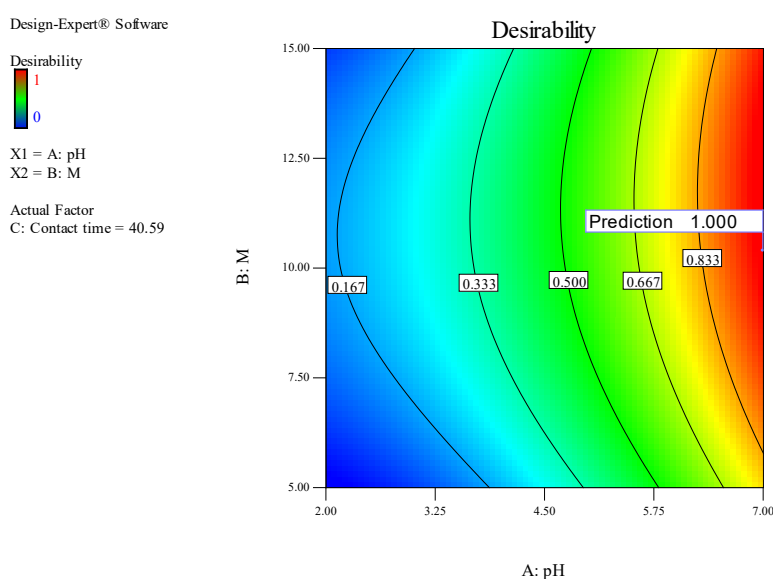


**Figure 14. The contours of desirability fluctuations**

## Adsorption mechanism

**Figure 15** shows the mechanism of  $\text{Hg}^{2+}$  adsorption onto the GO-CTS-PANI adsorbent. The figure shows that there are three main interactions between adsorbent and  $\text{Hg}^{2+}$  ions, which include: (1)- electrostatic interaction between dissociated carboxylic acid groups of GO and  $\text{HgOH}^+$  ions (Awad et al., 2020) (2)- soft-soft interaction between  $\text{Hg}^{2+}$  and sulfur atoms of CTS (Anirudhan et al., 2015; Gao et al., 2021; Santhana Krishna Kumar et al., 2013) and (3)- chelating interaction between N and  $\text{Hg}^{2+}$  (Zeng et al., 2019).

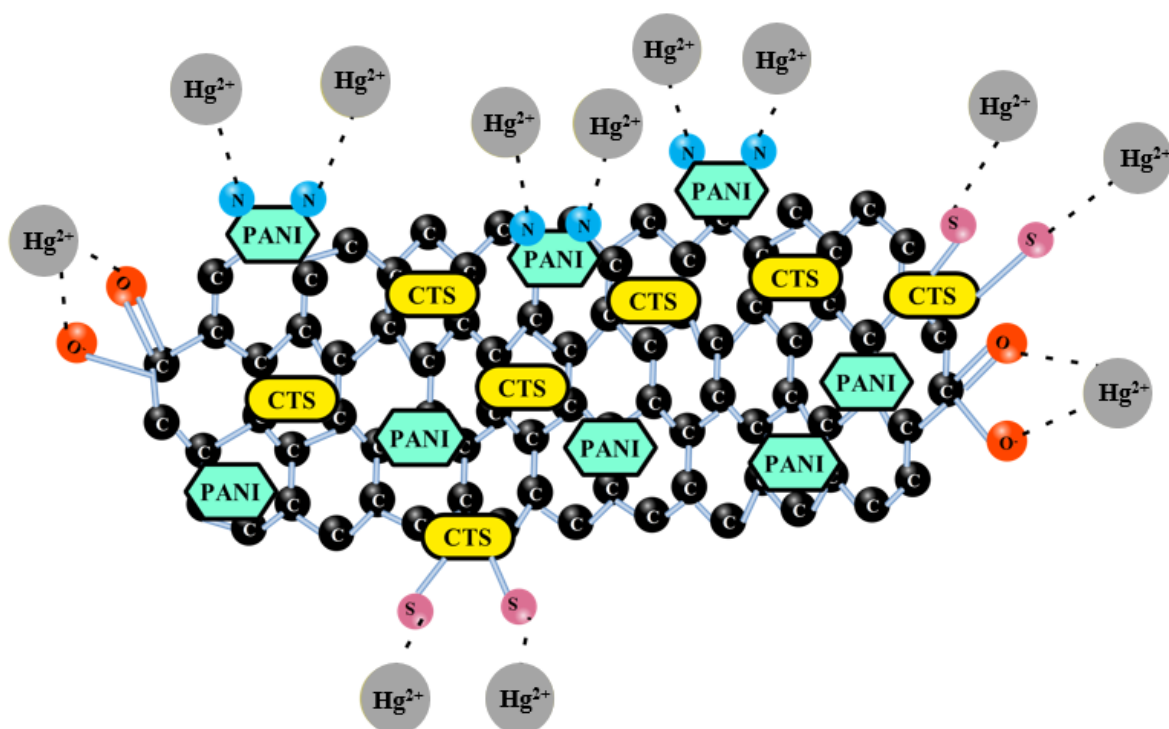


**Figure 15. Adsorption mechanism of  $\text{Hg}^{2+}$  on to the GO-CTS-PANI**

## Adsorption isotherm

To evaluate the adsorption mechanism and determine the dominance of Freundlich and Langmuir isotherms, two-parameter, and three-parameter equations (mentioned in **Figure 16**) were applied. In the first step, two-parameter calculations are analysed as shown in **Figure 16**.

The outcomes indicate that the regression coefficient of both isotherms was over 0.95 and the precise determination of the mechanism is simply not possible. Based on two-parameter relationships, the maximum absorption capacity ( $Q_{\max}$ ), Langmuir coefficient ( $K_{\text{ads}}$ ),  $K_f$  and  $n$  were estimated as 232.5 mg g<sup>-1</sup>, 6.76 L mg<sup>-1</sup>, 32.95 and 1.75, respectively. However, considering the three-parameter Sips, Khan and Toth isotherms ( $R^2$  more than 0.99) and modelling them in Curve Expert Professional software, it was revealed that the exponential coefficients of the models did not converge to 1. Consequently, the Freundlich isotherm was found to be superior (Eftekhari et al., 2020; Eftekhari et al., 2021). It was observed that Hg<sup>2+</sup> ions were adsorbed onto GO-CTS-PANI in some sequential layers and  $0 < 1/n < 1$  indicating a favourable adsorption process. **Figure 17** shows that in Temkin model,  $b < 8$  KJ mol<sup>-1</sup>, and according to the Dubinin-Radushkevich (D-R) equations,  $E < 8$  KJ mol<sup>-1</sup>. Therefore, the adsorption of Hg<sup>2+</sup> ions onto GO-CTS-PANI is physically in nature. The D-R isotherm model was used to calculate the  $Q_m$  and  $K$  factors which were found to be 102 mg g<sup>-1</sup> and 2E-07, correspondingly (Eftekhari et al., 2020).

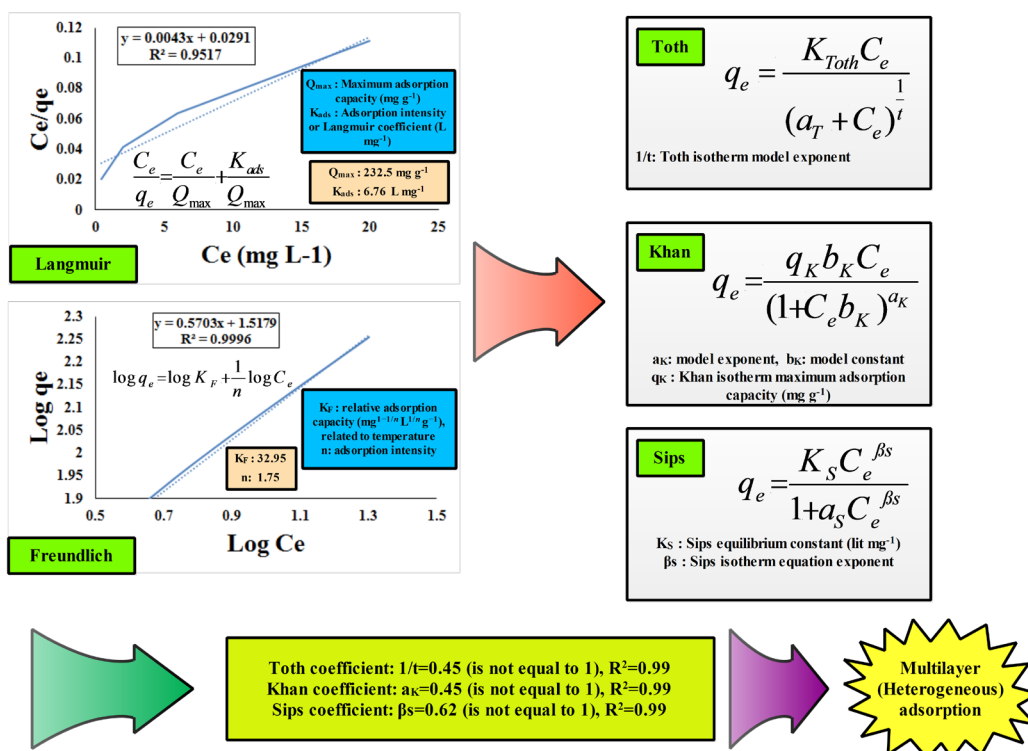


Figure 16. The computational model of  $\text{Hg}^{2+}$  adsorption onto GO-CTS-PANI.

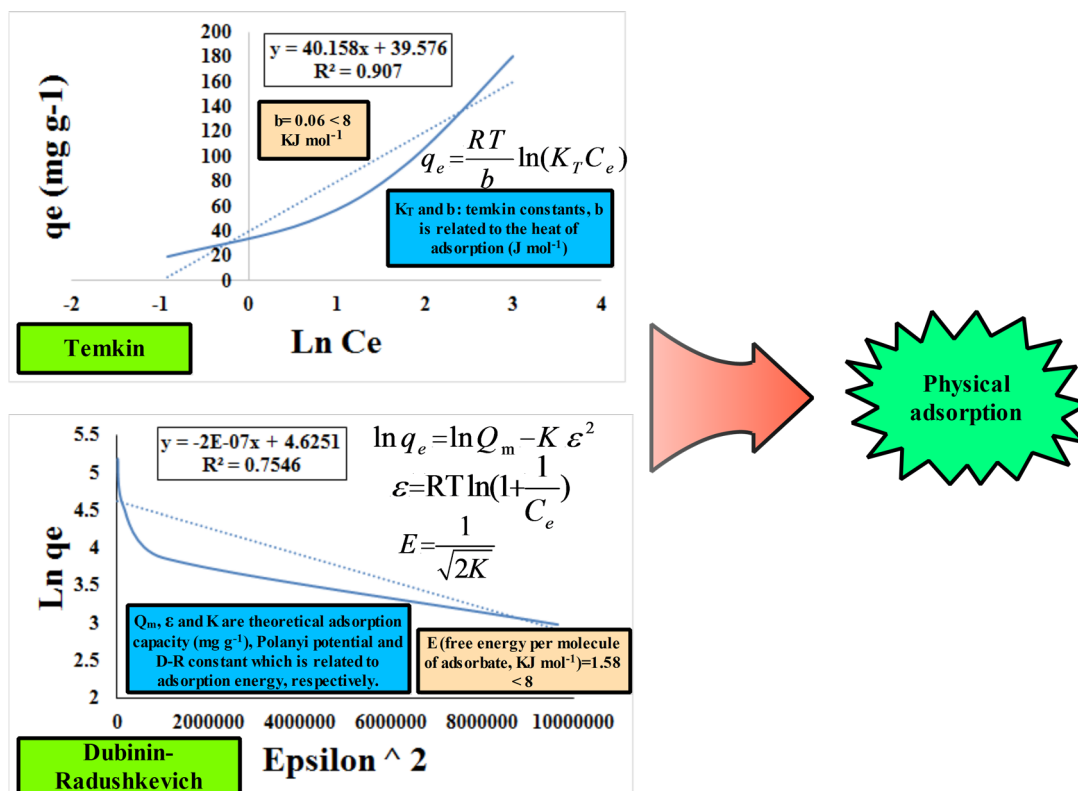
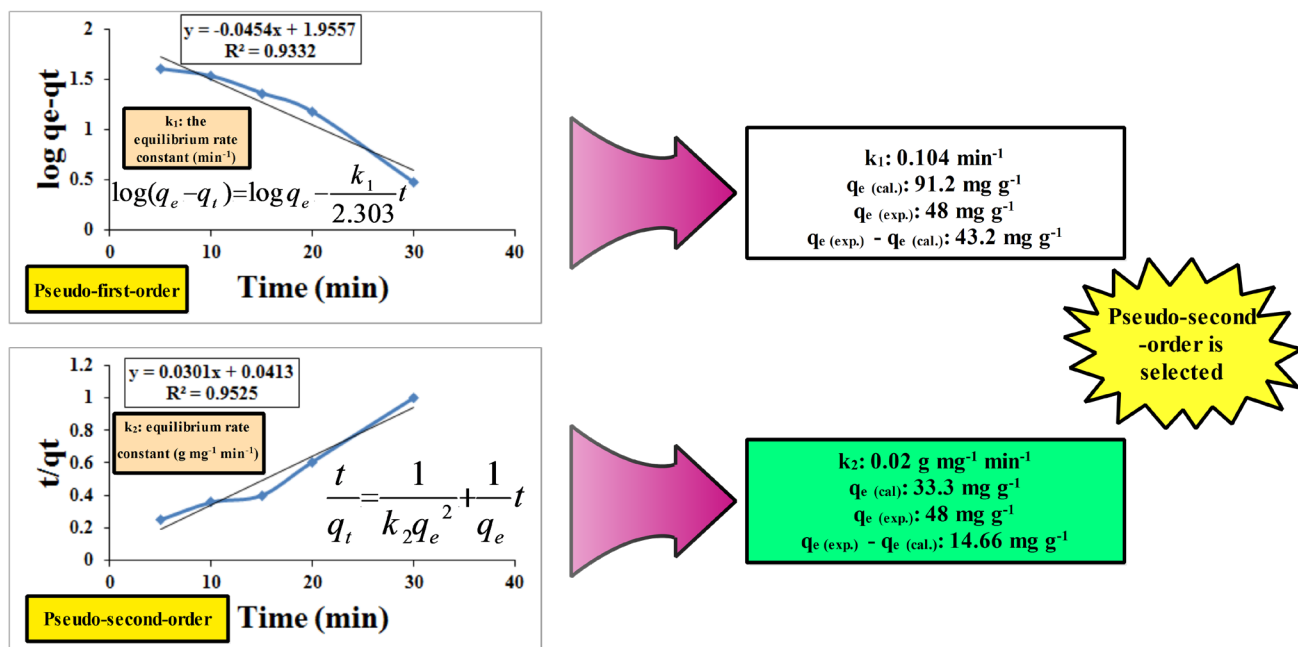


Figure 17. The physical, chemical, or intra-particle mechanism of  $\text{Hg}^{2+}$  adsorption onto GO-CTS-PANI.

## Adsorption kinetic

**Figures 18 and 19** demonstrate the results of  $\text{Hg}^{2+}$  kinetic adsorption onto GO-CTS-PANI using four models: Pseudo-First-Order (PFO), Pseudo-Second-Order (PSO), Intra-particle, and Elovich. Based on the data presented in **Figure 18**, the PSO model produced a more desirable  $R^2$  value and a smaller difference between experimental and calculated  $q_e$  values compared to the PFO model. Therefore, it can be concluded that the adsorption of  $\text{Hg}^{2+}$  onto the GO-CTS-PANI follows by the pseudo second order model with a rate of  $k_2=0.02 \text{ mg g}^{-1} \text{ min}^{-1}$  ( $R^2=0.95$ ) (Eftekhari et al., 2020; Eftekhari et al., 2021).



**Figure 18. The outputs of kinetic reaction order and coefficient calculations in this study**

**Figure 19** shows that it is evident that the kinetic behaviour of  $\text{Hg}^{2+}$  adsorption onto GO-CTS-PANI can be described by both Intra-particle ( $R^2=0.98$ ) and Elovich ( $R^2=0.94$ ) models. The Intra-particle kinetic curve has intercept of  $C=-20.6$  indicating that both integrated intra-particle and mass transfer mechanisms play a significant role in the adsorption process

(Eftekhari et al., 2020). Moreover, the Elovich model suggests that GO-CTS-PANI has a heterogeneous surface which is consistent with the results of isothermal assessments.

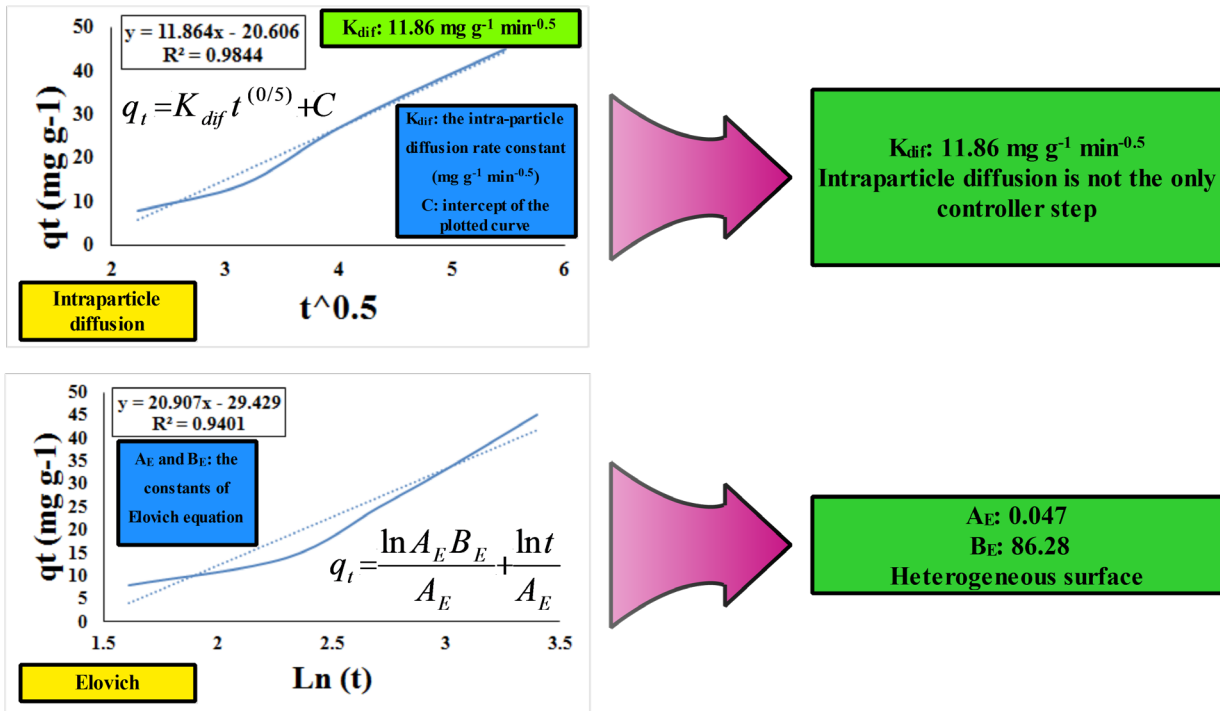


Figure 19. The outcomes of Elovich and Intra-particle kinetic models in the investigation.

## Machine learning

This study also utilised machine learning practices for two purposes: (1) to improve the accuracy of prediction parameters and (2) to establish an intelligent infrastructure for online investigation of purification systems using the adsorption method. The distribution of data used in the machine learning process, carried out using the RF method is illustrated in **Figure 20**.

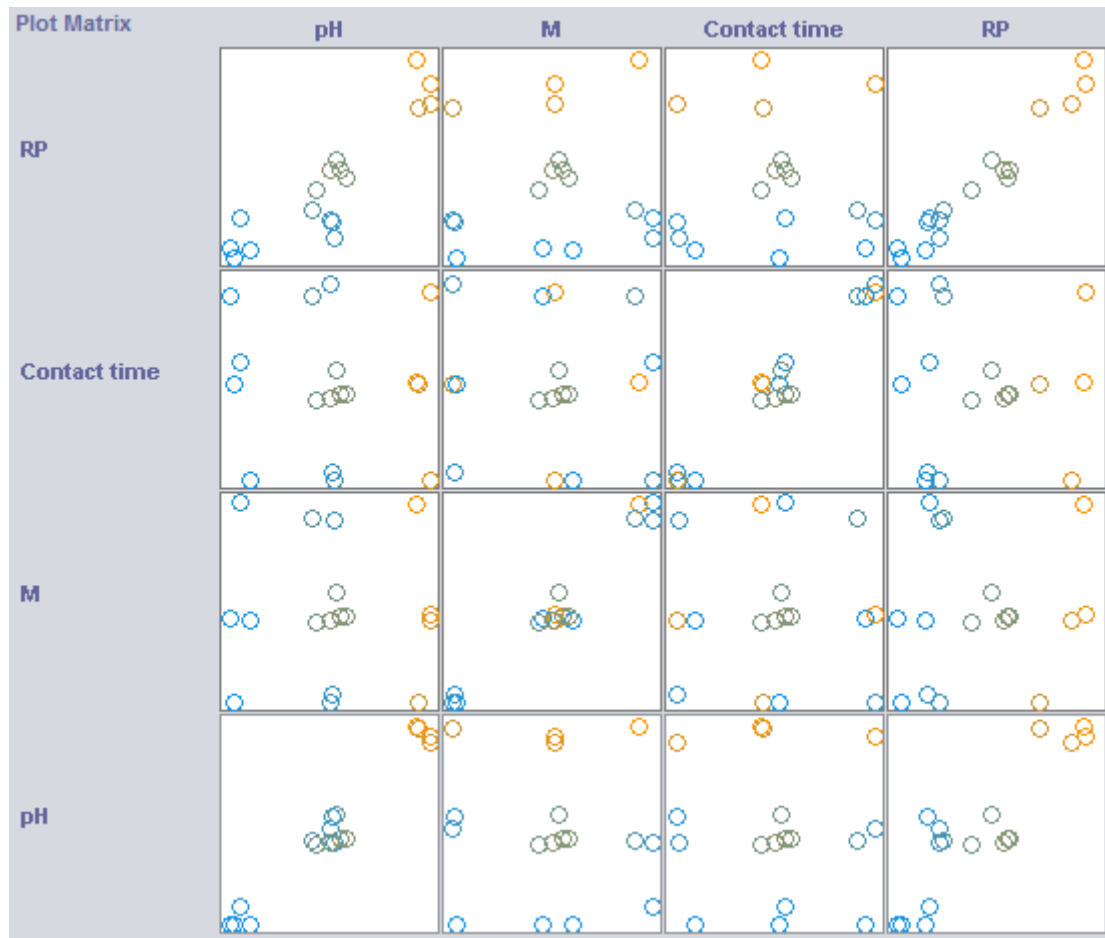
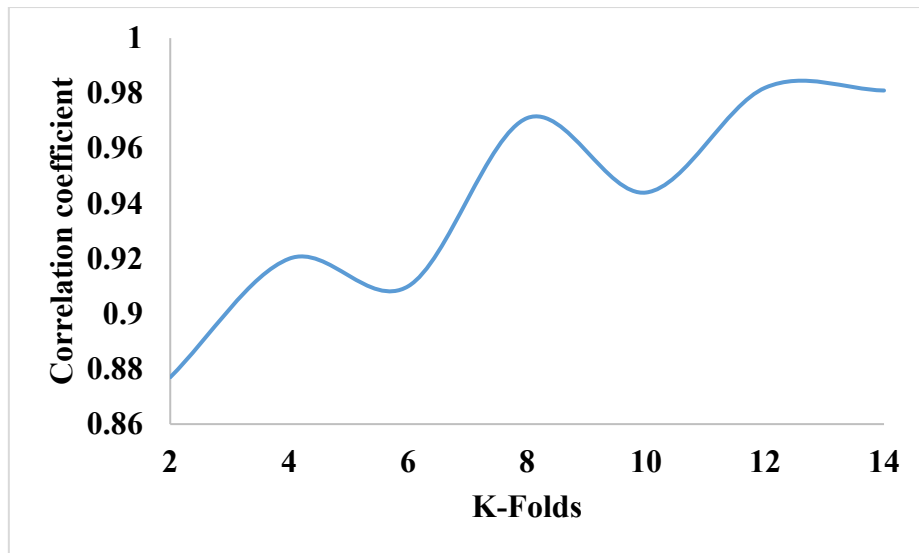
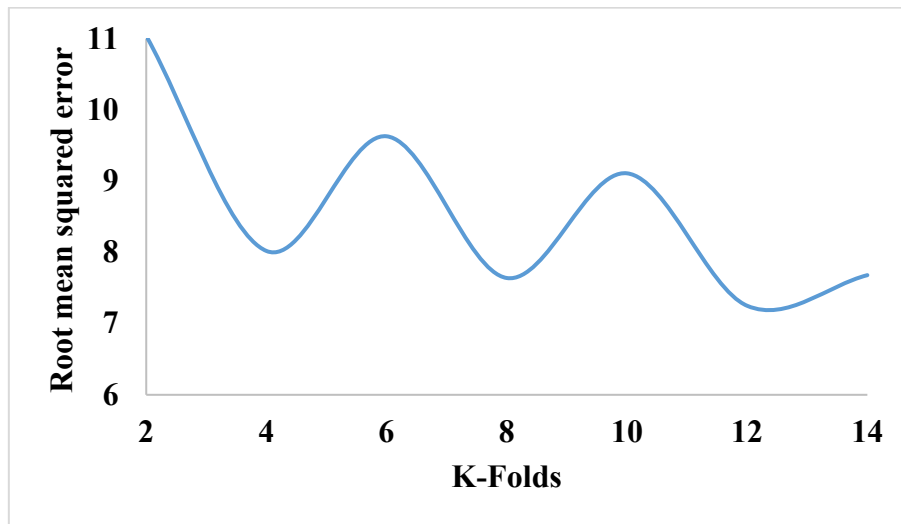


Figure 20. The distribution of data used for the machine learning modelling in this study.

Figure 21 displays the performance of the RF algorithm at different K-Folds Cross-Validation (KFCV) during training and testing process of the data. By adjusting the number of folds, the proportion of testing and training data can be determined. The correlation coefficient (Figure 21a) and root mean square error (Figure 21b) both indicate that the correlation coefficient generally increases as the number of folds increases but with some fluctuations in different steps. conversely, the behaviour of root mean square error is similar to correlation coefficient but in reverse. Therefore, the best condition is achieved at K=12 and the details are summarised in Table 5. It is worth noting that by applying the RF algorithm, the prediction performance is improved, and operation of the adsorption process can be managed automatically without the need for further examinations or other mathematical computations.



(a)



(b)

Figure 21. The effects of the number of K-folds on (a) correlation coefficient and (b) root mean square error

Table 5. The statistical indicators of the RF algorithm performance for K=12

Correlation coefficient	98.2%
Mean absolute error	6.16
Root mean square error	7.25
RAE	38.7%
RRSE	38.26%
Total Number of Instances	17



**Figure 22** show the scatterplot between observed and predicted values of the removal percentage (RP). It shows that the prediction process achieved high accuracy, providing evidence of the high validity of the RF algorithm for optimising the adsorption of  $\text{Hg}^{2+}$  ions onto GO-CTS-PANI nanocomposite. The development of a Decision Support Ssystem (DSS) for the prediction of  $\text{Hg}^{2+}$  purification from water resources by adsorption process is an important achievement, and the statistical outputs of the system are highly encouraging.

The system employs the RF algorithm and takes into account critical input variables, including contact time, the quantity of adsorbent, and pH. The notably high correlation coefficient of 98.2% signifies a robust positive connection between the input variables and the outcome variable, which, in this instance, pertains to the extent of  $\text{Hg}^{2+}$  removal. This strong correlation coefficient indicates that the input variables possess substantial predictive power regarding the outcome variable, a crucial characteristic of a dependable Decision Support System (DSS). Mean Absolute Error (MAE) and Root Mean Square Error (RMSE) represent two common metrics for gauging the accuracy of a prediction model. MAE reflects the average absolute disparity between predicted and actual values, while RMSE signifies the square root of the average squared difference between predicted and actual values. In this scenario, the MAE of 6.16 and the RMSE of 7.25 indicate that the DSS's predictions closely align with the actual values. These low values underscore the high precision and reliability of the system's predictions, a vital aspect for effective decision-making.

Furthermore, Relative Absolute Error (RAE) and Root Relative Square Error (RRSE) serve as supplementary metrics for assessing prediction model accuracy. RAE quantifies the average absolute discrepancy between predicted values and actual values, normalized by the average actual value, while RRSE denotes the square root of the average squared difference between predicted values and actual values, also normalized by the average actual value. In this context, the RAE of 38.7% and the RRSE of 38.26% are relatively elevated. This implies that there

exists some degree of error in the DSS's predictions. Nevertheless, it is essential to note that these values still fall within an acceptable range and do not diminish the overall reliability of the system.

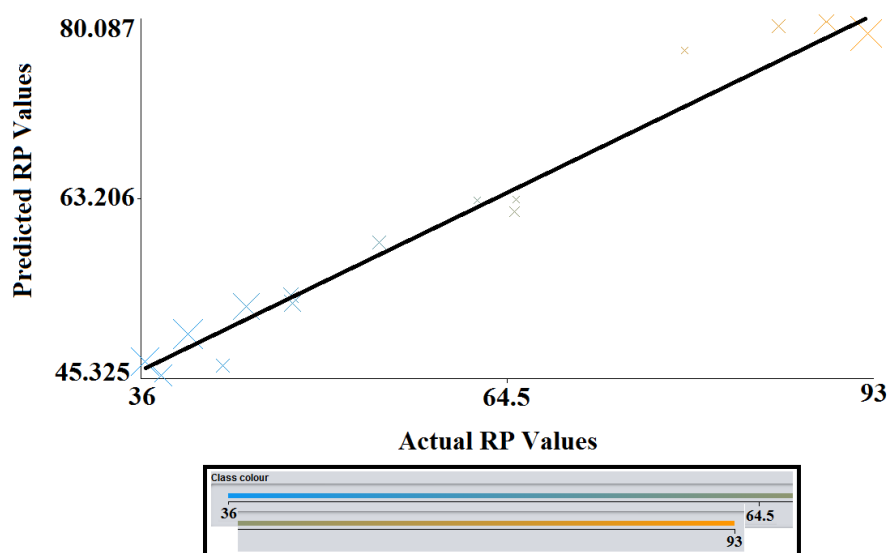


**Figure 22. The scatter plot between predicted and actual values of RP% in RF algorithm (K=12)**

### Test of Reusability

To evaluate the potential for reusing GO-CTS-PANI, we conducted five cycles of adsorption and desorption, employing a 0.1 mol L<sup>-1</sup> HCl (hydrochloric acid) solution for desorption. As depicted in **Figure 23**, following three rounds of utilizing the GO-CTS-PANI adsorbent, we observed only a marginal 6% decrease in removal percentage (RP). Nevertheless, in subsequent cycles, a more substantial reduction in RP became evident. Based on these observations, it can be inferred that GO-CTS-PANI remains effective for up to three cycles without a noteworthy decline in RP.

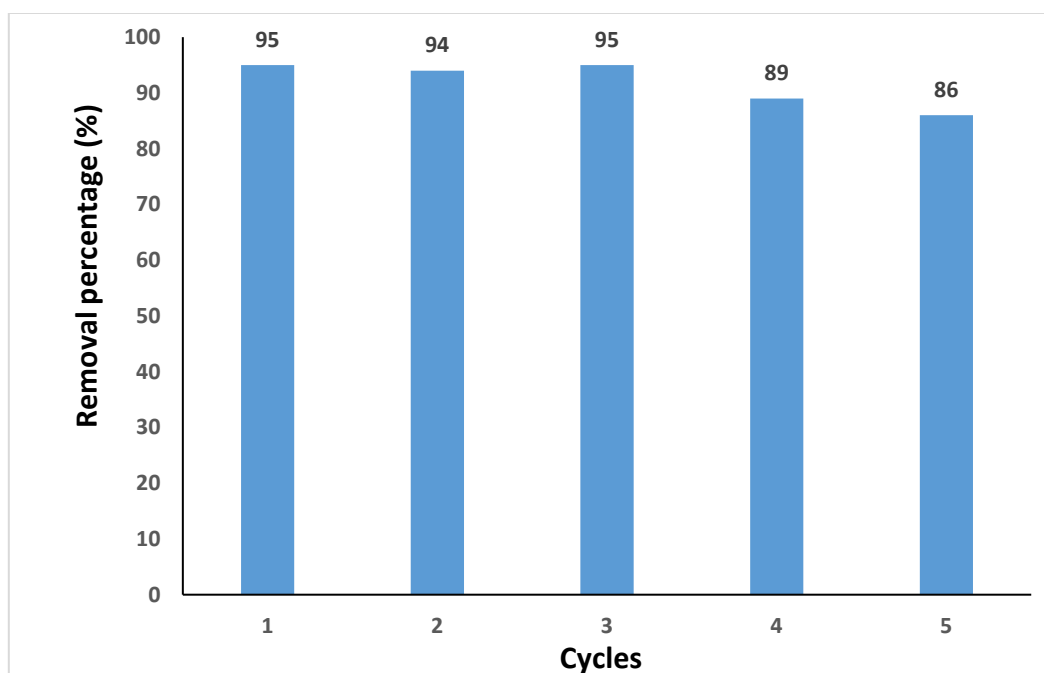


**Figure 23. Results of the reusability of GO-CTS-PANI nanocomposite**

### **Comparison with other studies**

Table 6 provides a comparison between the newly developed GO-CTS-PANI composite in this study and other adsorbents employed for  $\text{Hg}^{2+}$  removal. The findings clearly illustrate that this novel adsorbent exhibits a remarkable adsorption capacity for  $\text{Hg}^{2+}$  within a short timeframe. Furthermore, as it can be effectively reused for at least three cycles without a significant reduction in removal percentage, the GO-CTS-PANI composite can be considered a highly efficient adsorbent. According to the data in Table 6, it is evident that the GO-CTS-PANI composite outperforms other adsorbents, such as palm shell activated carbon modified with ionic liquids, in terms of adsorption capacity. This enhanced performance of the GO-CTS-PANI composite can be attributed to its advantageous functional groups, including the sulfur atoms found in CTS nanoplates, the presence of nitrogen atoms in PANI, and the electrostatic

interactions between the carboxylic acid groups of GO and  $\text{Hg}^{2+}$  ions. Consequently, these results strongly suggest that GO-CTS-PANI holds substantial promise as a material for effectively removing mercury from aqueous solutions.

**Table 6. Comparison between GO-CTS-PANI and other adsorbents for  $\text{Hg}^{2+}$  removal**

Adsorbent	Adsorption capacity (mg g <sup>-1</sup> )	Reference
2-mercaptobenzamide modified itaconic acid-grafted-magnetite nanocellulose composite	240.0	(Anirudhan and Shainy 2015)
Palm shell activated carbon impregnated with task-specific ionic-liquids	83.3	(Abu Ismaiel et al., 2013)
Polyamine modified reduced graphene oxide	63.8-59.9	(Yap et al., 2020)
Magnetic carbon nanotube	172.8	(Homayoon et al., 2017)
Mercapto-modified bentonite	19.3	(Sahan et al., 2018)
Mercaptobenzothiazole modified cellulose	204.1	(Krishna Kumar et al., 2013)
GO-CTS-PANI	232.5	This study

## Conclusions

The GO-CTS-PANI composite proved effective as an adsorbent for eliminating  $\text{Hg}^{2+}$  from water samples. The optimal conditions, resulting in a 95% removal rate for 50 mg L<sup>-1</sup>  $\text{Hg}^{2+}$ , were determined as follows: pH= 6.5, 12 mg of GO-CTS-PANI adsorbent, and a 30-minute contact period, employing the Box-Behnken method. The adsorption process exhibited a multilayer adsorption mechanism with physical interactions on the surface, as evident from conventional calculations. Kinetic analysis revealed that the adsorption reaction adhered to the PSO equation. Sensitivity analysis identified pH as the most influential factor impacting the adsorption process. Both RSM and machine learning techniques, specifically the RF method, proved effective for optimizing the adsorption process and predicting its efficiency, respectively. Furthermore, the GO-CTS-PANI nanocomposite demonstrated its reusability through five cycles of adsorption/desorption, with merely a 6% reduction in removal efficiency observed after three cycles. Ultimately, this study underscores the exceptional efficiency and

reusability of the GO-CTS-PANI composite as an adsorbent for Hg<sup>2+</sup> removal, showcasing its potential for future applications in water purification.

## References

Abu Ismaiel A, Kheireddine Aroua M, Yusoff R (2013) Palm shell activated carbon impregnated with task-specific ionic-liquids as a novel adsorbent for the removal of mercury from contaminated water. *Chem Eng J* 225: 306-314.

Amini-Fazl MS, Barzegarzadeh M, Mohammadi R (2021) Surface Modification of Graphene Oxide with Crosslinked Polymethacrylamide via RAFT Polymerization Strategy: Effective Removal of Heavy Metals from Aqueous Solutions. *J Inorg Organomet Polym* 31: 2959–2970.

Albatrni H, Qiblawey H, El-Naas MH (2021) Comparative study between adsorption and membrane technologies for the removal of mercury. *Sep Purif Technol* 257: 117833.

Anirudhan TS, Shainy F (2015) Effective removal of mercury(II) ions from chlor-alkali industrial wastewater using 2-mercaptobenzamide modified itaconic acid-grafted-magnetite nanocellulose composite. *J Colloid Interface Sci* 456: 22-31.

Arshad F, Selvaraj M, Zain J, Banat F, Abu Haija M (2019) Polyethylenimine modified graphene oxide hydrogel composite as an efficient adsorbent for heavy metal ions. *Sep Purif Technol* 209: 870-880.

Awad FS, AbouZied KM, Abou El-Maaty WM, El-Wakil AM, Samy El-Shall M (2020) Effective removal of mercury(II) from aqueous solutions by chemically modified graphene oxide nanosheets. *Arab J Chem* 13: 2659-2670.

538 Berg DM, Djemour R, Gütay L, Zoppi G, Siebentritt S, Dale PJ (2012) Thin film solar cells  
 539 based on the ternary compound Cu<sub>2</sub>SnS<sub>3</sub>. Thin Solid Films 520: 6291–6294.

540 Briffa J, Sinagra E, Blundell R (2020) Heavy metal pollution in the environment and their  
 541 toxicological effects on humans. Heliyon 6: e04691.

542 Eftekhari M, Akrami M, Gheibi M, Azizi-Toupkanloo H, Fathollahi-Fard AM, Tian G (2020)  
 543 Cadmium and copper heavy metal treatment from water resources by high performance  
 544 folic acid-graphene oxide nanocomposite adsorbent and evaluation of adsorptive  
 545 mechanism using computational intelligence, isotherm, kinetic, and thermodynamic  
 546 analyses. Environ Sci Pollut Res 27: 43999-44021.

547 Eftekhari M, Gheibi M, Azizi-Toupkanloo H, Hossein-Abadi Z, Khraisheh M, Fathollahi-Fard  
 548 AM, Tian G (2021) Statistical optimization, soft computing prediction, mechanistic and  
 549 empirical evaluation for fundamental appraisal of copper, lead and malachite green  
 550 adsorption. J Ind Inf Integr 23: 100219.

551 Gao P, Lei J, Tan J, Wang G, Liu H, Zhou L (2021) Self-assembled magnetic microcrystalline  
 552 cellulose/MoS<sub>2</sub>/Fe<sub>3</sub>O<sub>4</sub> composite for efficient adsorptive removal of mercury ions (Hg<sup>2+</sup>).  
 553 Compos Commun 25: 100736.

554 Ghadirimoghaddam D, Gheibi M, Eftekhari M (2023) Graphene oxide-cyanuric acid  
 555 nanocomposite as a novel adsorbent for highly efficient solid phase extraction of Pb<sup>2+</sup>  
 556 followed by electrothermal atomic absorption spectrometry; statistical, soft computing and  
 557 mechanistic efforts. Inter J Environ Anal Chem 103:469-490.

558 Global Mercury Assessment 2018. United Nation, Environmental Programme. **2019.**

559 Han Z, Guo Y, Yang W, Tang R, Wang H, Wu S (2020) Removal of mercury from flue gases  
 560 over iron modified activated carbon made by in situ ion exchange method. *J Energy Inst*  
 561 93: 1411-1418.

562 Homayoon F, Faghihian H, Torki F (2017) Application of a novel magnetic carbon nanotube  
 563 adsorbent for removal of mercury from aqueous solutions. *Environ Sci Pollut Res* 24:  
 564 11764–11778.

565 Jathar SB, Rondiya SR, Jadhav YA, Nilegave DS, Cross RW, et al., Ternary Cu<sub>2</sub>SnS<sub>3</sub>:  
 566 Synthesis, Structure, Photoelectrochemical Activity, and Heterojunction Band Offset and  
 567 Alignment. *Chem Mater* 33(6): 1983–1993.

568 Lei Y, Chen F, Luo Y, Zhang L (2014) Synthesis of three-dimensional graphene oxide foam  
 569 for the removal of heavy metal ions. *Chem Phys Lett* 593: 122-127.

570 Li L, Luo C, Li X, Duan H, Wang X (2014) Preparation of magnetic ionic  
 571 liquid/chitosan/graphene oxide composite and application for water treatment. *Int J Biol*  
 572 *Macromol* 66: 172-178.

573 Liu J, Duan Y, Song L, Zhang X (2018) Constructing sandwich-like polyaniline/graphene  
 574 oxide composites with tunable conjugation length toward enhanced microwave  
 575 absorption. *Org Electron* 63, 175-183.

576 Mbanga O, Ncube S, Tutu H, Chimuka L, Cukrowska E (2019) Mercury accumulation and  
 577 biotransportation in wetland biota affected by gold mining. *Environ Monit Assess* 191:  
 578 186.

579 Krishna Kumar AS, Kalidhasan S, Rajesh V, Rajesh N (2013) Adsorptive Demercuration by  
 580 Virtue of an Appealing Interaction Involving Biopolymer Cellulose and  
 581 Mercaptobenzothiazole. *Ind Eng Chem Res* 52: 11838–11849.

582 Raj D, Maiti SK (2019) Sources, toxicity, and remediation of mercury: an essence review.  
 583 Environ Monit Assess 191: 566.

584 Rezazadeh N, Danesh S, Eftekhari M, Farahmandzadeh M (2022a) Application of graphene  
 585 oxide and its derivatives on the adsorption of a cationic surfactant (interaction mechanism,  
 586 kinetic, isotherm curves and thermodynamic studies). J Mol Liq 368: 120720.

587 Rice KM, Walker EM, Wu M, Gillette C, Blough ER (2014) Environmental Mercury and Its  
 588 Toxic Effects. J Prev Med Public Health 47(2): 74–83.

589 Saadati T, Eftekhari M, Rezazadeh N, Nazarabad MK (2023) Graphene oxide–bismuth  
 590 tungstate (GO–Bi<sub>2</sub>WO<sub>6</sub>) nanocomposite as a green adsorbent for lead removal: isotherm,  
 591 kinetics and thermodynamic study. Int J Environ Sci Technol 20: 1301–1314.

592 Sahan T, Erol F, Yilmaz S (2018) Mercury(II) adsorption by a novel adsorbent mercapto-  
 593 modified bentonite using ICP-OES and use of response surface methodology for  
 594 optimization. Microchim J 138: 360-368.

595 Santana AJ, dos Santos WNL, Silva LOB, das Virgens CF (2016) Removal of mercury(II) ions  
 596 in aqueous solution using the peel biomass of *Pachira aquatica* Aubl: kinetics and  
 597 adsorption equilibrium studies. Environ Monit Assess 188: 293.

598 **Santhana Krishna Kumar A, Kalidhasan S, Rajesh V, Rajesh N (2013) Adsorptive**  
 599 **Demercuration by Virtue of an Appealing Interaction Involving Biopolymer Cellulose and**  
 600 **Mercaptobenzothiazole. Ind Eng Chem Res 52: 11838-11849.**

601 Shabani-Nooshabadi M, Zahedi F (2017) Electrochemical reduced graphene oxide-polyaniline  
 602 as effective nanocomposite film for high-performance supercapacitor applications.  
 603 Electrochim Acta 245: 575-586.



Streets DG, Devane MK, Lu Z, Bond TC, Sunderland EM, Jacob DJ (2011) All-Time Releases of Mercury to the Atmosphere from Human Activities. *Environ Sci Technol* 45: 10485–10491.

Tchounwou PB, Ayensu WK, Ninashvili N, Sutton D (2003) Environmental exposure to mercury and its toxicopathologic implications for public health. *Environ Toxicol* 18(3): 149-75.

Vasudevan S, Lakshmi J, Sozhan G (2012) Optimization of electrocoagulation process for the simultaneous removal of mercury, lead, and nickel from contaminated water. *Environ Sci Pollut Res* 19: 2734–2744.

Velempini T, Pillay K (2019) Sulphur functionalized materials for Hg(II) adsorption: A review. *J Environ Chem Eng* 7: 103350.

Wang C, Tian H, Jiang J, Zhou T, Zeng Q, He X, Huang P, Yao Y (2017) Facile Synthesis of Different Morphologies of Cu<sub>2</sub>SnS<sub>3</sub> for High-Performance Supercapacitors. *ACS Appl. Mater. Interfaces* 9 (31): 26038–26044.

Wei Y, Zhang Y, Gao X, Ma Z, Wang X, Gao C (2018) Multilayered graphene oxide membranes for water treatment: A review. *Carbon* 139: 964-981.

Yan X, Feng J, Li P, Li J, Ren B, Gao S, Cao R (2021) Fast and efficient removal of mercury ions using zirconium-based metal–organic framework filter membranes. *Inorg Chem Commun* 131: 108796.

Yap PL, Tung TT, Kabiri S, Matulick N, Tran DNH, Losic D (2020) Polyamine-modified reduced graphene oxide: A new and cost-effective adsorbent for efficient removal of mercury in waters. *Sep Purif Technol* 238: 116441.

626 Yu JG, Yue BY, Wu XW, Liu Q, Jiao FP, Jiang XY, Chen XQ (2016) Removal of mercury by  
627 adsorption: a review. Environ Sci Pollut Res 23: 5056–5076.

628 Zaman MB, Poolla R (2020) Morphological tuning of hydrothermally derived visible light  
629 active Cu<sub>2</sub>SnS<sub>3</sub> nanostructures and their applications in photocatalytic degradation of  
630 reactive industrial dyes. Opt Mater 104: 109853.

631 Zeng H, Wang L, Zhang D, Yan P, Nie J, Sharma VK, Wang C (2019) Highly efficient and  
632 selective removal of mercury ions using hyperbranched polyethylenimine functionalized  
633 carboxymethyl chitosan composite adsorbent. Chem Engin J 358: 253-263.

634

635

636

637

638

639

640

641

642

643

644

645

646

647

648

649 **Ethical approval**

650 Not applicable.

651 **Consent to participate**

652 Not applicable.

653 **Consent for publication**

654 Not applicable.

655 **Competing interests**

656 The authors declare no competing interests.

657 **Contributions**

658 Sara Enferadi: data curation, methodology; Mohammad Eftekhari: data curation, methodology,  
659 supervision, conceptualization, writing—review and editing; Mohammad Gheibi:  
660 methodology, software, writing—review and editing; Nikoo Nabizadeh Moghaddam: data  
661 curation, methodology; Stanislaw Wacławek: writing—review and editing, and supervision;  
662 Kourosh Behzadian: data curation and conceptualization, supervision, writing—review and  
663 editing.

664 **Funding**

665 There is no funding for this research.

666

667